Tectonics

RESEARCH ARTICLE
10.1029/2018TC004981

Key Points:
- In the inner zone of the Chos Malal FTB, the Cordillera del Viento was slowly cooled since at least 70 Ma
- Basement-involved thrusting has occurred at ~15–7 Ma in both the inner and outer sectors of the FTB and at ~9–7 Ma at its front
- The Chos Malal FTB was formed by a normal sequence of deformation propagation from the Late Cretaceous at least the latest Miocene

Supporting Information:
- Supporting Information S1

Correspondence to:
N. P. Sánchez,
natalia.sanchez@uns.edu.ar

Citation:
Sánchez, N. P., Coutand, I., Turienzo, M., Lebinson, F., Araujo, V., & Dimieri, L. (2018). Tectonic evolution of the Chos Malal fold-and-thrust belt (Neuquén Basin, Argentina) from (U-Th)/He and fission track thermochronometry. *Tectonics*, *37*. https://doi.org/10.1029/2018TC004981

Received 19 JAN 2018
Accepted 11 MAY 2018
Accepted article online 6 JUN 2018

Tectonic Evolution of the Chos Malal Fold-and-Thrust Belt (Neuquén Basin, Argentina) From (U-Th)/He and Fission Track Thermochronometry

N. P. Sánchez[1], I. Coutand[2], M. Turienzo[1], F. Lebinson[1], V. Araujo[1], and L. Dimieri[1]

[1]Universidad Nacional del Sur, Instituto Geológico del Sur (INGEOSUR), CONICET, Departamento de Geología, Bahía Blanca, Argentina, [2]Dalhousie University, Department of Earth Sciences, Halifax, Nova Scotia, Canada

Abstract In the southern central Andes at 37–38°S latitude, the Chos Malal fold-and-thrust belt (FTB), which results from the Late Cretaceous closure of the Neuquén Basin, has generated increasing interest because of its potential for hydrocarbon exploration. Using detailed field mapping, seismic reflection, and well data analysis, we have produced balanced cross sections, which combined with apatite and zircon (U-Th)/He, and fission track thermochronology from samples distributed along the FTB, bring new constraints on the chronology of the structural development of the Chos Malal FTB. Fully reset samples obtained from the Early Jurassic rocks at the bottom of the sedimentary sequence exposed in the Cordillera del Viento, a major basement-involved hinterland structure, permit to quantify its cooling rate from 5.4 ± 4.1 and 3.8 ± 3.2 °C/Ma between 70 and 55 Ma down to between 2.0 ± 1.3 and 1.3 ± 0.9 °C/Ma after 55 Ma until the present. Detrital apatite fission track ages from Late Jurassic and Early Cretaceous sandstones reveal that tectonically driven exhumation through basement-involved thrusting has occurred at ~15–7 Ma in both the inner and outer sectors of the FTB. Finally, the cooling and exhumation of the Las Yeseras-Pampa Tril basement-involved anticlines at the mountain front at ~9–7 Ma, slightly younger than previously assumed, suggests a normal sequence of faulting propagation. Our proposed thermostructural model of the Chos Malal FTB contributes to a better understanding of the tectonic evolution of this segment of the Andes.

1. Introduction

The Chos Malal fold-and-thrust belt (FTB), a segment of the southern central Andes located in the Argentinian province of Neuquén at 37–38°S latitude (Figure 1), results from the Late Cretaceous to Neogene closure of the Neuquén Basin. Although there is an increasing interest for better constraining Andean tectonics and petroleum systems development in this area, there is lack of consensus on the timing, style, and amount of deformation of the Chos Malal FTB. This study focuses on quantifying the activity, through time, of the major structures in the Chos Malal FTB to constrain the spatial and temporal tectonic evolution and identify the processes responsible for its development.

There is general agreement that most of the contractional deformation in the Chos Malal FTB appears to have happened during two major stages, of Late Cretaceous-Paleogene and Neogene ages (Cobbold & Rossello, 2003; Folguera et al., 2007, 2015; Kozlowski et al., 1998; Ramos & Kay, 2006; Rojas Vera et al., 2015; Sagripanti et al., 2016; Vergani et al., 1995). However, the timing, distribution, and magnitude of either stage remain controversial. The older contractional stage covers a broad time interval of 60 Ma, between 100 and 40 Ma. The onset of deformation is proposed to have occurred during the deposition of the latest Cretaceous Neuquén Group (Figure 2) synchronously with the onset of the Andean orogeny, ~100 Ma ago (Fennell et al., 2015; Tunik et al., 2010), and is suggested to have lasted until the syntectonic emplacement of the subvolcanic bodies of the Sierra del Mayal dated with ^{39}Ar-^{40}Ar on andesite whole rock at 39.7 ± 0.2 Ma (Cobbold & Rossello, 2003; Figure 2). Some authors proposed to divide this period into two different events, one during the Upper Cretaceous and another during the Paleocene-Eocene (Cobbold & Rossello, 2003; Sagripanti et al., 2016, and references therein).

The second stage of deformation is thought to have occurred during the middle Miocene and is interpreted to have caused the structural development of the Chos Malal FTB between 15 and 12 Ma (Folguera et al., 2007). This time interval is constrained by the ages and crosscutting relationships of the youngest folded volcanic rocks dated at 14.5 ± 0.1 Ma using ^{40}Ar-^{39}Ar on amphibole (Spagnuolo et al., 2012) and of the Cerro Negro andesite dated by U-Pb on zircons at 11.63 ± 0.20 Ma and 11.55 ± 0.06 Ma (Gürer et al., 2016).

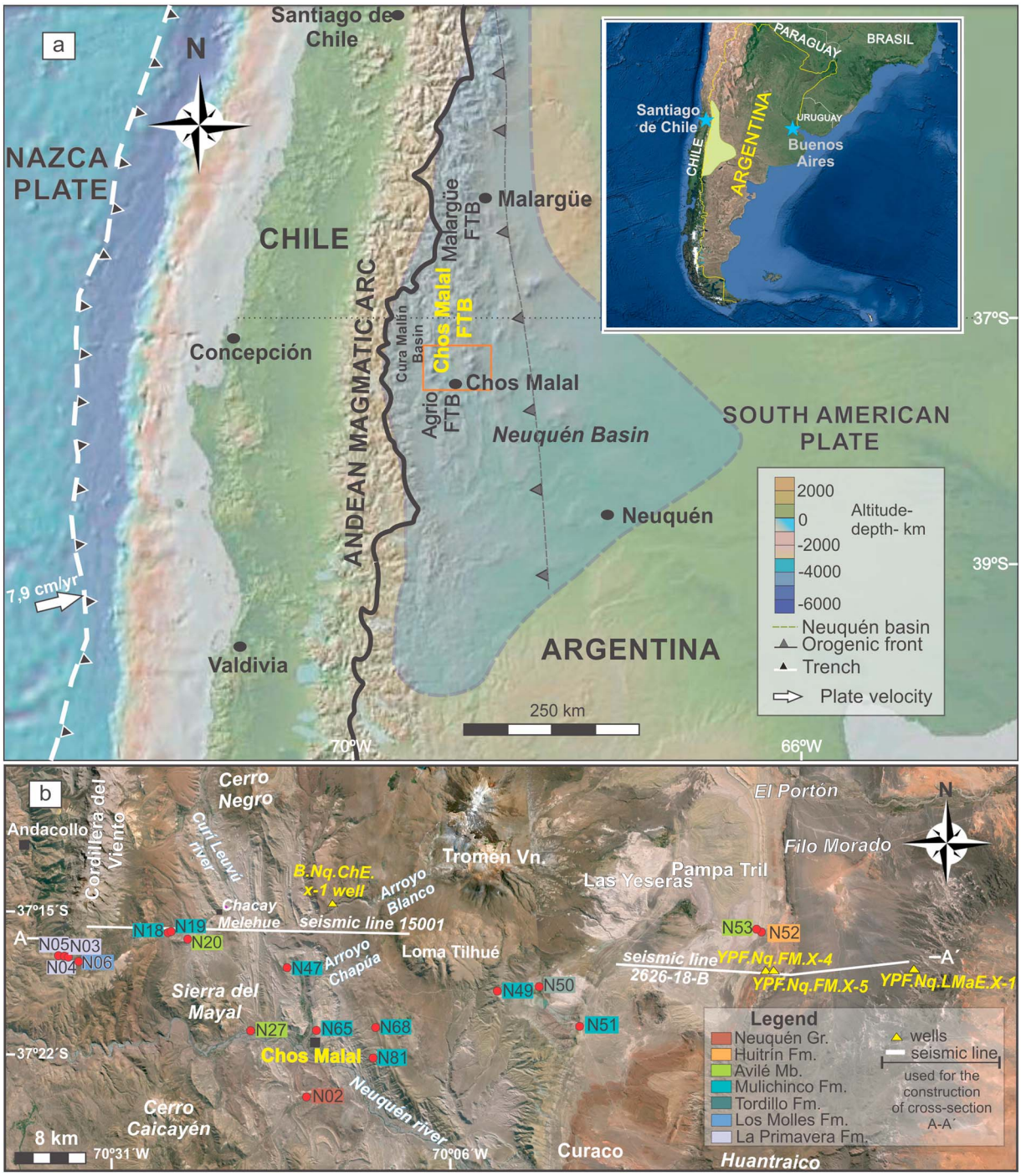

Figure 1. (a) Shuttle Radar Topography Mission image (SRTM, 90 m) showing the location of the Chos Malal fold-and-thrust belt (FTB) in the northern part of Neuquén province (Argentina), which formed as the result of the subduction of Farallón and Nazca plates underneath the South American plate. The red square indicates the location of Figure 1b. (b) Landsat image of the study transect. Colored rectangles indicate the location and the stratigraphic units in which samples were collected for apatite fission track (AFT) apatite (U-Th)/He (AHe) and zircon (U-Th)/He (ZHe) thermochronology.

After that episode, it is considered that the Chos Malal FTB has remained tectonically inactive (Folguera et al., 2007; Gürer et al., 2016).

The aim of this paper is to reconstruct the Late Cretaceous to present structural and thermal development of the Chos Malal FTB, at 37°18′S latitude, between the Cordillera del Viento to the west and the Andean deformation front (Filo Morado; Figures 1b and 2a). The style of deformation was characterized by conducting

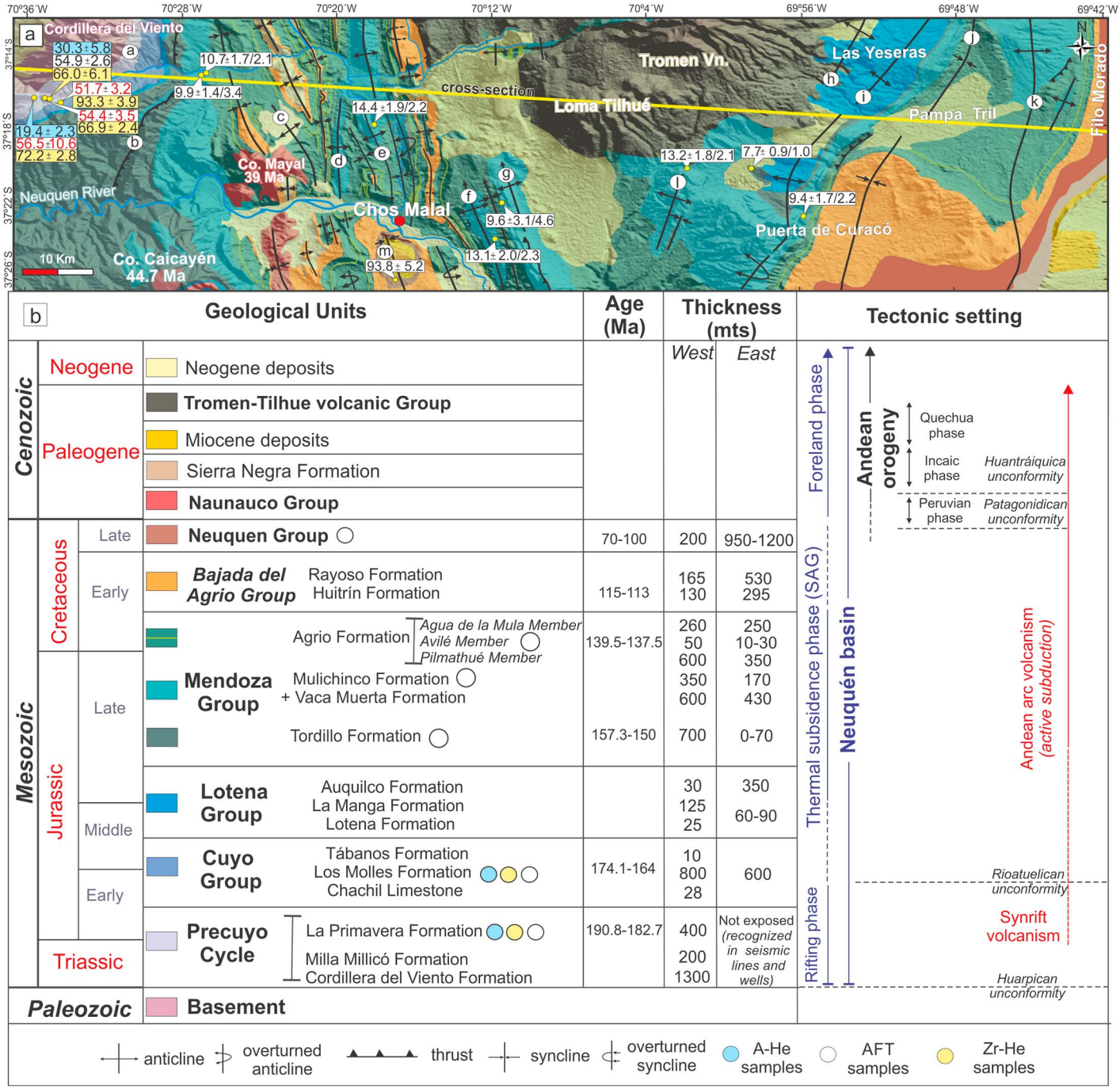

Figure 2. (a) Geological map of the Chos Malal FTB after our own observations and modified from Sánchez (2015) and Sánchez et al. (2015). The samples dated using apatite AHe ages are in light blue, AFT ages are in white, and ZHe ages are in yellow. Numbers in red are AFT pooled ages and associated 1σ error for samples passing the χ^2 test ($P(\chi^2) > 5\%$ in Table 2). The other black numbers in white boxes indicate the AFT ages and associated 95% confidence level errors of the youngest populations extracted with the software *Binomfit* (Brandon, 1992, 1996, 2002) from the samples failing the χ^2 test ($P(\chi^2) < 5\%$ in Table 5. Black letters in white circles correspond to structures that are a = Cordillera del Viento, b = El Alamito back thrust, c = Mayal anticline, d = Chos Malal anticline, e = Las Máquinas anticline, f = West Tilhué anticline, g = East Tilhué anticline, h = Totoras anticline, i = Las Yeseras anticline, j = Las Yeseras syncline, k = Pampa Tril anticline, l = Chacayco anticline, and m = Truquico syncline. (b) Stratigraphic and ages, nature, and thicknesses of the different geological units preserved in the Neuquén Basin. The column to the right indicates the geodynamic settings in which the Neuquén Basin evolved through time. For explanations and references, see text.

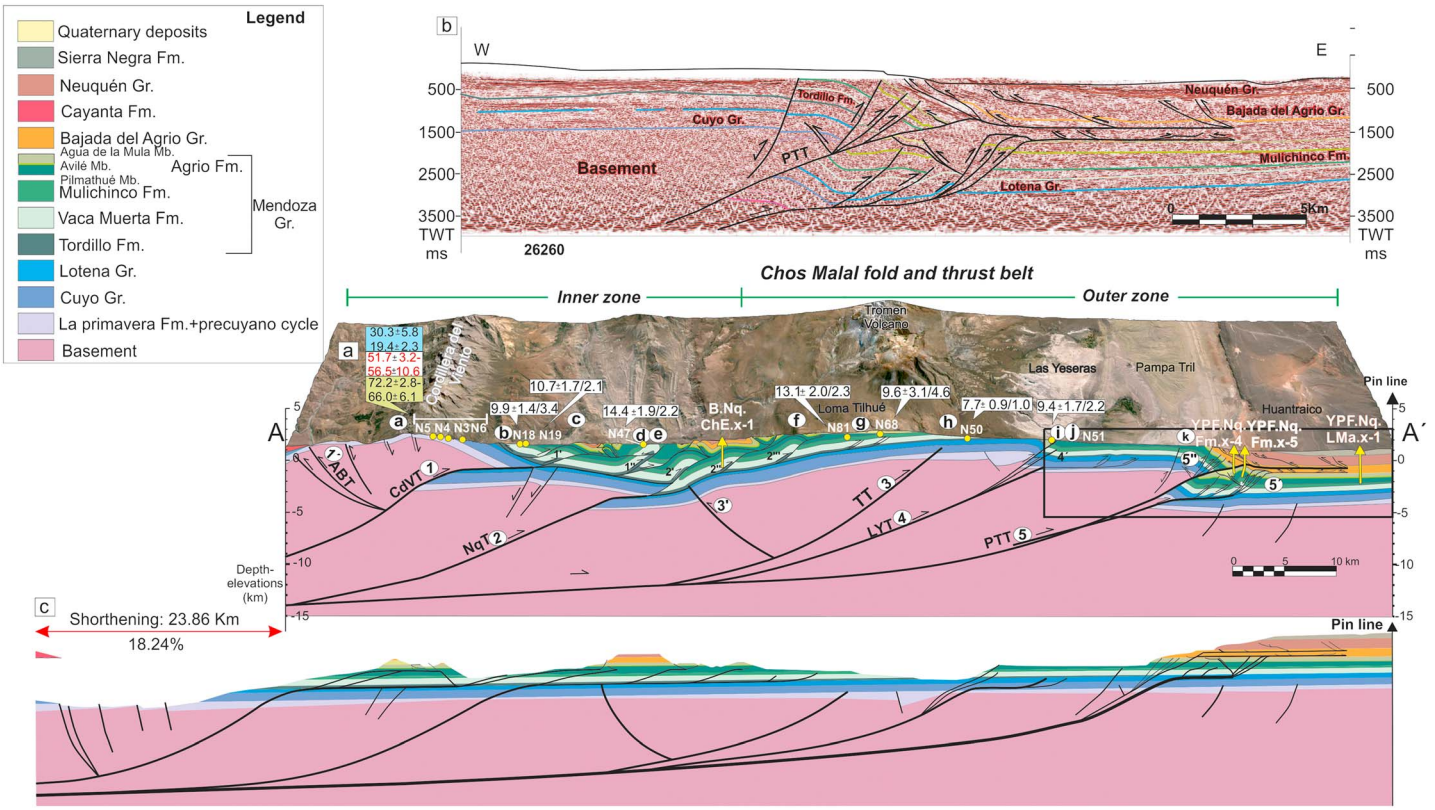

Figure 3. (a) Structural cross section across the Chos Malal FTB. Abbreviations are ABT: Andacollo back thrust; CdVT: Cordillera del Viento thrust; NqT: Neuquén thrust; TT: Totoras thrust; LYT: Las Yeseras thrust; and PTT: Pampa Tril thrust. Wells are yellow triangles and thermocronologic data, and the black letters (a–k) are the same as in Figure 2. (b) Seismic profile 26260 line drawings interpretation (for location, see Figure 1a). (c) Restored cross section showing a horizontal shortening of 23.9 km (18.2%).

detailed field mapping and analyzing ~75 km of seismic reflection data correlated with four exploratory wells (Figure 1b) in order to produce a 107-km-long regional-scale transect (Figures 2 and 3). Eighteen rock samples distributed along the transect including the Early Jurassic synrift sequences and the entire Mesozoic-Cenozoic stratigraphic succession exposed in the FTB yielded grains of adequate size, quality, and quantity for apatite fission track (AFT) dating. Furthermore, four samples were processed for zircon (U-Th)/He (ZHe) and two for apatite (U-Th)/He (AHe) dating (Table 1). This new data set allows us to reconstruct the low-temperature cooling history of the region and contribute to better constrain the timing of activity of the main structures exposed along the transect. We have integrated the thermochronological data to balance and retrodeform the cross section to quantify the amount of crustal shortening since the Late Cretaceous. This analysis of the sequential development of the tectonic structures highlights the relationships between thick-skinned and thin-skinned structures of the Chos Malal FTB. Our new kinematic model for the development of the Chos Malal FTB improves knowledge on the orogenic building of the Neuquén Andes.

2. Geological Setting

The geological history the southern central Andes involves several tectonic, sedimentary, and magmatic cycles, which from the Paleozoic to the present have produced a complex morphotectonic configuration along the southwestern margin of Gondwana (Ramos et al., 2014; Ramos & Folguera, 2005; Ramos & Kay, 2006). The oldest units in the study area are exposed west of the Cordillera del Viento, and they include carboniferous metasedimentary rocks (Zöllner & Amos, 1973) and Permian granitoids (Llambías et al., 2007), which constitute the basement of the Neuquén Basin in this region (Figure 2). A rifting episode affected these basement rocks during the Late Triassic-Early Jurassic, creating numerous NW-SE trending half-grabens (Vergani et al., 1995). Synrift volcaniclastic sequences, known as "precuyano" (Gulisano et al., 1984), include

Table 1
Sample Identification and Location

Sample	Unit	Longitude (W)	Latitude (S)	Elevation (m)	AFT	AHe	ZHe
N2	Neuquén Gr.	37°26′3.7″	70°17′9.7″	910	✓	x	x
N52	Huitrín	37°17′38.08″	69°41′26.20″	924	✓	x	x
N53	Avilé	37°17′31.56″	69°41′42.36″	931	✓	x	x
N20	Avilé	37°15′54.00″	70°25′30.04″	1,110	✓	x	x
N27	Avilé	37°21′45.36″	70°21′3.96″	888	✓	x	x
N18	Mulichinco	37°15′27.36″	70°26′57.16″	1,114	✓	x	x
N19	Mulichinco	70°26′47.08″	37°15′23.08″	1,100	✓	x	x
N47	Mulichinco	37°18′3.28″	70°18′2.16″	1,155	✓	x	x
N49	Mulichinco	37°20′19.36″	70°1′54.16″	1,579	✓	x	x
N51	Mulichinco	37°22′45.12″	69°55′49.08″	1,265	✓	x	x
N65	Mulichinco	37°21′58.32″	70°16′1.56″	993	✓	x	x
N68	Mulichinco	37°22′4.08″	70°11′30.12″	1,367	✓	x	x
N81	Mulichinco	37°23′56.04″	70°11′48.48″	1,223	✓	x	x
N50	Tordillo	37°20′11.04″	69°58′44.08″	1,445	✓	x	x
N6	Los Molles	37°16′48.9″	70°34′0.2″	1,506	✓	x	✓
N3	La Primavera	37°16′ 30.1″	70°34′54.04″	1,510	✓	✓	✓
N4	La Primavera	37°16′28.1″	70°35′5.8″	1,494	✓	x	✓
N5	La Primavera	37°16′25.03″	70°35′40.6″	1,464	✓	✓	✓

the Cordillera del Viento, Milla Millicó, and La Primavera formations (Figure 2b). These deposits are exposed on the eastern flank of the Cordillera del Viento and preserve a complex architecture and variable stratigraphic thicknesses controlled by normal faults (Sagripanti et al., 2014). During the Early-Middle Jurassic, subduction initiated along the western Gondwana margin (Franzese et al., 2003) and by the Late Jurassic the Andean magmatic arc was fully developed (Charrier et al., 2007; Ramos, 2010). Afterward, a stage of widespread thermal subsidence in the back-arc region dominated the basin evolution during the rest of the Jurassic and the Early Cretaceous (Arregui et al., 2011; Vergani et al., 1995). From the Middle Jurassic, several transgressive and regressive cycles were responsible for the deposition and distribution of hydrocarbon source rocks, reservoirs, and seals in the sedimentary sequence (Vergani et al., 2011) and were separated into three main Groups. The Cuyo Group begins with the Chachil limestone (Figure 2b), which was dated at 185.7 ± 0.4 Ma based on zircon U-Pb ages of interlayered ashes (Leanza et al., 2013). It is overlain by the 800-m-thick Los Molles Formation, one of the source rocks of the Neuquén Basin, composed of black shales with high organic content interbedded with turbiditic sandstones. These rocks were deposited between the middle Pliensbachian and the early Bajocian (~186–170 Ma) as determined by ammonites, bivalves, and microfossils biozones (Gulisano & Gutiérrez Pleimling, 1995). The deposition of evaporites of the Tábanos Formation marks the end of the first marine cycle in the basin. A second marine cycle, from Middle Callovian to Late Oxfordian (~164–157 Ma; Gulisano et al., 1984) led to the deposition of the Lotena Group (Figure 2b), which comprises continental and platform sandstones of the Lotena Formation, limestones of the La Manga Formation, and evaporites of the Auquilco Formation (Zöllner & Amos, 1973). The Mendoza Group represent a third depositional cycle and starts with continental deposits of the Tordillo Formation of Kimmeridgian-Tithonian age as determined by detrital zircon U-Pb dating (Naipauer et al., 2015). This formation can reach 700 m thick in the western region, thinning to50 m in the east. It is overlain by the Late Jurassic-Early Cretaceous Vaca Muerta Formation starting with deep marine shales, which are the main source rocks of hydrocarbons in the Neuquén Basin (Figure 2b). This unit is overlain by the Mulichinco Formation (~139.5–137.5 Ma, 350–170 m thick) composed of continental to marine sandstones progressively transitioning to the marine dark shales and limestones of the Pilmathué Member (600–350 m thick) of the Valanginian-Barremian Agrio Formation. The latter continues with the Avilé Member 50–10 m thick composed of fluvial and eolian sandstones, which constitute one of the most important hydrocarbon reservoirs of the basin and with marine shales and limestones of the Agua de la Mula Member (260 m thick). Toward the end of the Early Cretaceous the basin shifts into a continental environment with the deposition of fluvial-eolian sandstones at the base of the Huitrín Formation, which are followed by evaporites and carbonates that represent the last connection of the Neuquén Basin with the proto Pacific Ocean (Leanza, 2003). The overlying Rayoso Formation contains dominantly fluvio-lacustrine deposits. The Huitrín and Rayoso formations constitute the Bajada

del Agrio Group, assigned to the Middle Barremian-Albian (127–101 Ma) according to biostratigraphic indicators (Aguirre-Urreta et al., 2008; Leanza, 2003). During the latest Cretaceous, the Neuquén depocenter evolved into a foreland basin with contractional tectonics prevailing in response to an increased rate of convergence between the Nazca and South American plates and the shallowing of the Waditi-Benioff zone (Ramos, 1998; Ramos & Folguera, 2005). According to Tunik et al. (2010) and Di Giulio et al. (2012), the unconformable deposition of sandstones, mudstones, and conglomerates of the Neuquén Group on top of the Mesozoic units results from this new tectonic setting (Figure 2) and marks the onset of contractional deformation in this sector of the Andes.

A magmatic activity, mostly of intermediate composition, took place during the Paleogene as represented by the Naunauco Group, which comprise the Colipili (intrusive) and the Cayanta (effusive) Formations (Cobbold & Rossello, 2003; Franchini et al., 2003; Llambías & Rapela, 1989; Zamora Valcarce et al., 2007). The best outcrops of these units are located in the Cerro Mayal, Cerro Caycayén, and west of the Cordillera del Viento in the Andacollo region (Figure 2).

The Neogene-present period is represented by the Miocene back-arc volcanic rocks exposed in the Sierra de Huantraico (Figure 1b), belonging to the Sierra Negra Formation and interlayered with clastic Cenozoic deposits (Garrido et al., 2012). In the study area, synorogenic deposits related to the Miocene contractional tectonics have been included in the Chos Malal Formation, which contains continental clastic sediments unconformably resting on deformed Mesozoic rocks (Cervera & Leanza, 2009). The youngest geological units of the study area are Holocene and Pleistocene rhyolites and andesites erupted from the Tilhue-Tromen Complex (Llambías et al., 2011) under a tectonic regime still debated: extensional (Folguera et al., 2008; Ramos & Folguera, 2005), contractional (Galland et al., 2007; Messager et al., 2010), or contractional with limited amounts of strike-slip displacements (Sagripanti et al., 2015).

3. Structure of the Chos Malal Fold-and-Thrust Belt

3.1. Methods

We have conducted detailed structural analysis and geological mapping, reported these field data on Google Earth images and digital elevation models (AsterGDEM) with 30-m resolution, to produce a new regional-scale geological map and a new balanced cross section modified from Sánchez (2015) including the structures located east of the Tromen Volcano (Figure 2a). We have constructed a 107-km-long regional cross section extending from the Cordillera del Viento to the frontal tip of the FTB in the Filo Morado region (Figures 1b and 3a) using two seismic reflection profiles (lines 15011 and 26260) and four 1.2- to 3-km-depth exploratory wells (Figure 1b) combined with structural field data. The depth to the detachment for the interpreted basement-involved structures was inferred to lie between 11 and 13 km, taking into account the potential location of the brittle-ductile transition in the upper crust, and according to one seismic event recorded by the Instituto Nacional de Prevención Sísmica with the hypocenter located at a depth of 10 km, showing that this deep faulting system is still active. The balanced cross section was constructed according to classical concepts of the geometric models of fault-related folds (e.g., Erslev, 1991; Mitra, 1990; Suppe, 1983; Suppe & Medwedeff, 1990). The restoration was carried out using the method of conservation of the length of lines (Dahlstrom, 1969), by measuring the top of the more competent Mesozoic units. The thickness of the sedimentary sequences increases gradually from east to west, and we used averaged values from field data in the western region and from well data in the eastern one. In order to unravel the sequential development of the structures, we constructed a forward model using *Fault-Fold-Forward* (Allmendinger, 2012). This software allowed us to make a balanced reconstruction of the FTB structures, combining fault-bend folds over flat-ramp-flat thrust geometries and trishear fault propagation folds, and to estimate the amount of horizontal shortening for each deformational stage. *Fault-Fold-Forward*, however, has some limitations in that it cannot reproduce multibend kink fault-bend folds because kink axes, due to the active ramp, do not refract across higher level inactive ramps and thus bed thickness is not preserved across higher ramps (Allmendinger, 2012). In this work, we used an apical angle of the trishear zone of 60° for all the structures and chose, based on the geometry of the folds, propagation versus displacement ratio (p/s) of 1.5.

3.2. Results

The Chos Malal FTB is a thick-skinned orogenic wedge, which can be divided into two discrete regions (Figure 3a): (1) the inner zone located between the Cordillera del Viento and the Tromen Volcano and (2)

the outer zone located between the Tromen Volcano and the orogenic deformation front. This structural configuration of the Chos Malal FTB is characterized by large-scale basement-involved folds located in the inner zone, as in the Cordillera del Viento where Paleozoic rocks are exposed, and in the outer zone where subsurface basement uplifts are recognized through wells and seismic lines in the region of Las Yeseras-Pampa Tril. The main basement-involved structures have a dominant eastward vergence, with subordinate development of back thrusts in the hanging walls, and generate a complex thin-skinned deformation in their leading edges characterized by fault-related folds on various scales and with NS to NNW oriented axial planes affecting the Mesozoic units of the Neuquén Basin. Our cross section integrates structures previously identified in the inner FTB by Sánchez (2015) and Sánchez (2015) with structures observed across the outer FTB to the east (Figures 1b and 3a).

The westernmost structure of the Chos Malal FTB is the Cordillera del Viento (labeled a in Figures 2a and 3a), a large fault-bend fold made of Paleozoic and Triassic igneous rocks, and developed in the hanging wall of the Cordillera del Viento thrust (CdVT) (labeled 1 in Figure 3a), which roots on the lower detachment at about 13 km depth and flattens upward into the evaporites of the Auquilco Formation (Lotena Group, Figure 3a). In the western foothills of the Cordillera del Viento, Paleogene volcanic rocks of the Cayanta Formation rest unconformably over the basement and Mesozoic rocks affected by the Andacollo blind back thrust (ABT; labeled 1′ in Figure 3a). The ABT has previously been interpreted as an inverted normal fault (Cobbold & Rossello, 2003; Zapata et al., 1999). In the Cordillera del Viento itself, Sagripanti et al. (2014) have mapped east dipping normal faults, bounding the synrift deposits (Precuyo Cycle) and associated these faults with moderate inversion. In order to produce enough structural relief to account for the angular unconformity observed below the Paleogene rocks, we interpret the ABT as a shortcut fault derived from the pre-Andean Mesozoic extensional system. The eastern flank of the Cordillera del Viento forms an east dipping homoclinal sequence (~30°–40°E) involving the whole Triassic-Cretaceous succession, interpreted as the forelimb of a large basement-involved fault-bend anticline (Kozlowski et al., 1996, 1998, related to the CdVT at depth. Horizontal shortening transmitted by the CdVT is accommodated by a large number of second-order structures involving the entire Mendoza Group, such as the Alamito back thrust and the Mayal, Chos Malal, and Las Máquinas anticlines (labeled b, c, d, and e in Figures 2a and 3a). Associated with these folds, there are structures of third- and fourth-order involving the Agrio Formation and younger units, within which are prominent repetitions of the Avilé Member (Turienzo et al., 2014). A second basement thrust sheet was recognized at depth from seismic profile 15011 (Turienzo et al., 2014) associated with the Neuquén thrust (NqT, labeled 2 in Figure 3a). As a result of the insertion of this fault into the sedimentary cover, several thin-skinned anticlines and synclines have developed in Loma Tilhué and nearby areas (labeled f and g in Figures 2a and 3a).

In the outer sector of the Chos Malal FTB, significant contractional structures previously recognized by Ploszkiewicz and Viñes (1987), Ramos and Barbieri (1989), Viñes (1989), Nocioni (1996), Kozlowski et al. (1998), Zapata et al. (2001), Allmendinger et al. (2004), and Zamora Valcarce et al. (2006) are associated with important hydrocarbon traps (Figure 3a). The structural configuration of the outer sector is related to the basement-involved Totoras, Las Yeseras, and Pampa Tril east verging thrusts (TT, LYT, and PTT, labeled 3, 4, and 5 in Figure 3a). The Totoras thrust shows limited displacement in the cross section, but farther north, it produces an east vergent anticline cored by Jurassic shales of Los Molles Formation (labeled h in Figure 2 a; Gulisano & Gutiérrez Pleimling, 1995). The second basement thrust sheet includes the Las Yeseras anticline (labeled i in Figure 2a), an eastward vergent asymmetric fold with a long, gently dipping backlimb and a short, steeply dipping forelimb, which we interpret as an incipient fault-bend-fold that has evolved into a fault propagation fold (labeled 4′ in Figure 3a). The final displacement along the structure has exposed the Auquilco Formation evaporites of the uppermost Lotena Group.

The PTT is the easternmost basement-involved structure, and it has a high level of structural complexity (labeled 5 in Figure 3a). The Pampa Tril anticline (labeled k in Figures 2a and 3a) has initiated as a fault-bend fold with an upper detachment in the evaporites of the Auquilco Formation (uppermost Lotena Group). Displacement along this horizon has created second-order structures in the sedimentary cover, such as the Filo Morado anticline (labeled 5′ in Figure 3a), which constitutes one of the most important oil traps in the area. This anticline has a double vergence with steeply dipping limbs, as confirmed by data from numerous wells, and consequently, it is not observed on seismic data (Zamora Valcarce et al., 2006; Zapata et al., 2001). The combination of a back thrust with minor thrusts in both flanks makes the Filo Morado anticline a pop-up

structure (Figure 3a). An out-of-sequence upper branch of the PTT generated a structural step of more than 3 km between the basement in the core of the Pampa Tril anticline and the basement underneath the undeformed foreland (labeled 5″ in Figure 3a). Sedimentary strata in the hanging wall are folded due to the upward propagation of this fault, which reaches an upper detachment level along the evaporites of the Bajada del Agrio Group. As postulated originally by Ploszkiewicz and Viñes (1987), the large eastward displacement on this thrust is balanced by the development of a passive roof back thrust (or underthrust), forming a triangle zone (Figures 3a and 3b). A set of minor back thrusts rises from this detachment, folding the overlying Late Cretaceous rocks.

Interpretation and analysis of the structural cross section point to a close relationship between basement-involved and sedimentary cover structures. The horizontal shortening calculated from the restoration of this cross section, with a pin line located at the forelandward extremity of the section, is 23.9 km, which amounts to 18.2% of its initial length (Figure 3c).

4. Apatite Fission Track and (U-Th)/He Thermochronology

4.1. Principles

Numerous studies have established the utility of apatite fission track (AFT) thermochronology and (U-Th)/He dating on apatite (AHe) and zircon (ZHe) to reconstruct the thermal history of upper crustal rocks and ultimately provide indirect information on the timing of brittle deformation (e.g., Reiners et al., 2018; Reiners & Brandon, 2006, and references therein).

The AFT method is based on the spontaneous decay of ^{238}U, into two positively charged nuclei repelling each other in opposite directions and leaving behind their trajectory an ionized trail in the crystal lattice called a fission track (Fleischer et al., 1975). Fission tracks are unstable features that shorten (anneal) by thermal and time-dependent recrystallization processes (e.g., Wagner & Van den haute, 1992). In apatite crystals, tracks are annealed at temperatures above 150°–120 °C, depending on the cooling rate and the composition of the crystal (e.g., Green et al., 1985; Ketcham et al., 1999; Reiners & Brandon, 2006). Determining the density of spontaneous fission tracks and the concentration of ^{238}U yields a single-grain fission track age (e.g., Donelick et al., 2005; Naeser, 1976; Tagami & O'Sullivan, 2005). Over geological timescales, significant track shortening occurs in fluorine-rich apatite between 60° and 110 °C (e.g., Donelick et al., 1999; Laslett et al., 1987; Laslett & Galbraith, 1996); this temperature range is called the partial annealing zone (Gleadow & Duddy, 1981; Green et al., 1986).

(U–Th)/He thermochronology is based on the decay of ^{235}U, ^{238}U, ^{232}Th, and ^{147}Sm by alpha emission (^{4}He nucleus; e.g., Hurley & Goodman, 1941; Farley, 2002). At temperatures lower than the effective closing temperature of given crystals, that is 70 ± 20 °C for apatite (e.g., Shuster et al., 2006; Wolf et al., 1998) and 180 ± 20 °C for zircon (e.g., Reiners et al., 2004), ^{4}He is mostly retained in the crystal lattice and a geologically meaningful cooling age can be calculated. When temperature increases, a variable fraction of ^{4}He can diffuse out of the crystal by thermally activated solid-state diffusion in a partial retention zone defined by approximate temperature range of 40–85 °C for apatite (Wolf et al., 1998) and 120–200 °C for zircon (Reiners, 2005; Reiners et al., 2018).

4.2. Methods

Along our structural transect, 26 samples of medium-grained sandstones, 6–10 kg in weights, were collected within La Primavera, Los Molles, Tordillo, Mulichinco, Agrio (Avilé Member), Huitrín, and Chos Malal Formations (Figures 1b and 2b), representing the entire stratigraphic column preserved in the basin from the oldest (Early Jurassic) to present-day deposits (Figure 2a and Table 2). Furthermore, we have spatially focused the sample collection in the vicinity of the most prominent tectonic structures including Cordillera del Viento, Mayal, Las Máquinas, Tilhue, Las Yeseras, and Pampa Tril (a, c, e, f, i, and k in Figure 2a), in order to detect temperature-time perturbations due to displacements related to their activity. In the laboratory, bulk samples were separated and prepared using a standard analytical procedure as described in Coutand et al. (2016). Detailed analytical procedures for both fission track and (U-Th)/He dating methods are provided in S1 and S2 in the supporting information.

Out of the 26 samples collected, only 18 yielded sufficient material to process AFT analyses. Between 7 and 60 grains (maximum datable number of grains per mount) were dated for each sample (Table 2), and each

Table 2
Apatite Fission Track Results

Sample	Latitude (S)	Longitude (W)	Stratigraphic unit	Stratigraphic age (Ma)	N° of grains	Spontaneous track density $\rho s \times 10^6$ cm^{-2} (Ns)	Induced track density $\rho i \times 10^6$ cm^{-2} (Ni)	Dosimeter track density $\rho d \times 10^6$ cm^{-2} (Nd)	P (χ^2)	Pooled age ± 1σ	U (ppm)	Number of confined track lengths	Mean track length (±1σ) (μm)	Mean track length SDT (μm)	Dpar (μm)
N2	37°26′3.7″	70°17′9.7″	Neuquén Gr.	~100–70	41	0.2369 (570)	0.5075 (1221)	1.1073 (3735)	0.4	95.0 ± 5.2	66	1	15.2	-	3.3
N52	37°17′38.08″	69°41′26.20″	Huitrín	[115–113]	16	0.3683 (322)	2.3666 (2069)	1.4003 (3523)	0.0	37.8 ± 2.4	22	2	13.3 ± 2.2	3.1	2.1
N53	37°17′31.56″	69°41′42.36″	Avilé	[133.8–132.5]	15	0.2192 (223)	2.1964 (2234)	1.4003 (3523)	6.1	24.3 ± 1.7	19	1	7.2	-	1.8
N20	37°15′54.00″	70°25′30.04″	Avilé	[133.8–132.5]	60	0.3566 (1619)	1.9977 (9070)	1.4003 (3523)	0	43.4 ± 4.8	20	16	10.5 ± 0.4	1.5	2.4
N27	37°21′45.36″	70°21′3.96″	Avilé	[133.8–132.5]	43	0.7079 (1643)	3.0183 (7005)	1.4003 (3523)	0	56.9 ± 2.1	27	27	12.1 ± 1.2	3.4	1.5
N18	37°15′27.36″	70°26′57.16″	Mulichinco	[139.5–137.5]	53	0.2162 (759)	3.1031 (10896)	1.4003 (3523)	0	16.9 ± 0.7	29	8	12.6 ± 0.9	2.6	1.5
N19	70°26′47.08″	37°15′23.08″	Mulichinco	[139.5–137.5]	26	0.2832 (340)	4.8125 (5777)	1.4003 (3523)	0	14.3 ± 0.8	43	2	11.6 ± 1.2	0.3	1.8
N47	37°18′3.28″	70°18′2.16″	Mulichinco	[139.5–137.5]	53	0.1541 (486)	2.2770 (7181)	1.4003 (3523)	0.3	16.5 ± 0.8	45	10	10.7 ± 1.3	4.0	2.0
N49	37°20′19.36″	70°1′54.16″	Mulichinco	[139.5–137.5]	58	0.3619 (942)	5.4263 (14126)	1.4003 (3523)	0.1	16.2 ± 0.6	52	3	6.5 ± 1.1	1.9	1.8
N51	37°22′45.12″	69°55′49.08″	Mulichinco	[139.5–137.5]	35	0.2167 (364)	3.5200 (5946)	1.4003 (3523)	0.0	14.9 ± 0.8	34	1	13.3	1.8	2.0
N65	37°21′58.32″	70°16′1.56″	Mulichinco	[139.5–137.5]	41	0.5203 (1458)	2.2802 (6390)	1.4003 (3523)	0	47.1 ± 1.7	25	20	11.4 ± 1.2	3.4	2.1
N68	37°22′4.08″	70°11′30.12″	Mulichinco	[139.5–137.5]	25	0.1957 (218)	2.7779 (3095)	1.4003 (3523)	0	17.1 ± 1.2	28	1	13.9	-	3.1
N81	37°23′56.04″	70°11′48.48″	Mulichinco	[139.5–137.5]	59	0.2886 (569)	3.3510 (6606)	1.4003 (3523)	0	21.0 ± 1.0	34	1	13.6	-	2.2
N50	37°20′11.04″	69°58′44.08″	Tordillo	[~157.3–150.0]	43	0.2052 (358)	4.4756 (7810)	1.4003 (3523)	0.1	11.2 ± 0.6	43	9	12.7 ± 1.2	3.4	2.1
N6	37°16′48.9″	70°34′0.2″	Los Molles	[174.1–166.1]	15	0.7471 (367)	3.1087 (1527)	1.1664 (3735)	30.3	51.7 ± 3.2	357	9	12.2 ± 0.4	1.1	2.5
N3	37°16′30.1″	70°34′54.04″	La Primavera	[190.8–182.7]	20	0.8595 (680)	3.2434 (2566)	1.1242 (3735)	0.1	54.9 ± 2.6	420	-	-	-	2.84
N4	37°16′28.1″	70°35′5.8″	La Primavera	[190.8–182.7]	12	1.5875 (335)	6.1460 (1297)	1.1453 (3735)	91.5	54.4 ± 3.5	695	-	-	-	2.6
N5	37°16′25.03″	70°35′40.6″	La Primavera	[190.8–182.7]	7	0.1513 (36)	0.5715 (136)	1.1580 (3735)	97.4	56.5 ± 10.7	69	-	-	-	3.5

Note. Abbreviations are N, number of individual grains dated per sample; ρ_s, spontaneous track density; ρ_i, induced track density; N_s, number of spontaneous tracks counted; N_i, number of induced tracks counted; ρ_d, induced track density in external detector adjacent to dosimetry glass; N_d, number of tracks counted in determining ρ_d; and P (χ^2), χ^2 probability.

single-grain age distribution was decomposed using the binomial peak method (Figure 4; Galbraith & Green, 1990) incorporated into the *Binomfit* program (Brandon, 1992, 1996, 2002) to identify discrete populations subsequently referred to as P_1 to Pn, the age of the populations increasing with n. Confined horizontal track lengths, angles between the confined tracks and the crystallographic C axis, and etch pit diameters (Dpar; Donelick et al., 1999) were also measured (Table 2).

The general crystallographic formula of the apatite is $Ca_5(PO_4)_3(OH, F, Cl)$, with hydroxi-apatite ($Ca_5(PO_4)_3(OH)$), fluorapatite ($Ca_5(PO_4)_3F$), and chloro apatite ($Ca_5(PO_4)_3Cl$) as end-members. Small compositional variations can produce important changes in the annealing kinetics of apatite grains (e.g., Barbarand et al., 2003; Carlson et al., 1999; Green et al., 1986). To track these changes, we have measured Ca, F, Cl, P, Ce, La, Sr, Fe, Mn, Si, and Na in 547 dated grains at the Robert M. MacKay Electron Microprobe Laboratory (Department of Earth Sciences, Dalhousie University). Because of the lack of straightforward relationships between our single-grain ages and elemental compositions, we provide our compositional results in the supporting information (S3).

Four and two samples located at the bottom of the stratigraphic section were processed for ZHe and AHe dating, respectively. Four zircon aliquots (Table 3) and five apatite aliquots (Table 4) were selected and processed for each sample.

4.3. AFT Results

The distribution of fission track grain ages (FTGA) generally shows a wide range, from 1.5 Ma to 202 Ma, with pooled ages ranging between 11.2 ± 0.6 and 95.0 ± 5.2 Ma (Tables 2 and 5). Most of the samples (except N4, N5, N6, and N53) fail the χ^2 test (Galbraith, 1981; Green, 1981) with P (χ^2) <5% (Table 2 and Figure 4) indicating that FTGA distributions are nonpoissonian and represent a mixture of components or peak ages (Brandon, 1992, 1996, 2002). Six age components were defined in our data set (Table 5). Except for the four basal samples, the rest show a wide range of single-grain ages. Samples N50, N68, N51, N19, and N18 show a population P_1 with ages in the range of 10.7 ± 1.7/2.1 Ma to 7.7 ± 0.9/1.0 Ma with no particular upward trend in the section (Table 5). Samples N50, N81, N49, and N47 of the Tordillo and Mulichinco Formations have an older population between 15.0 ± 1.4/3.2 Ma and 13.1 ± 2.0/2.3 Ma, grouped in P_2 (Table 5 and Figure 4). Components P_3 to P_6 representing older peak are present throughout the entire stratigraphic column (Table 5 and Figure 4).

A total of 115 confined horizontal track lengths were measured in the sample set (Table 2). However, the inability to know both the track length distribution in the grains when they entered the basin and were deposited and the low-number of tracks measured in each sample (between 1 and 27 tracks) prevents us from drawing meaningful conclusions about the mean track length distributions and drastically limits the usefulness of this part of our data set in that respect. Three samples distributed in the stratigraphic

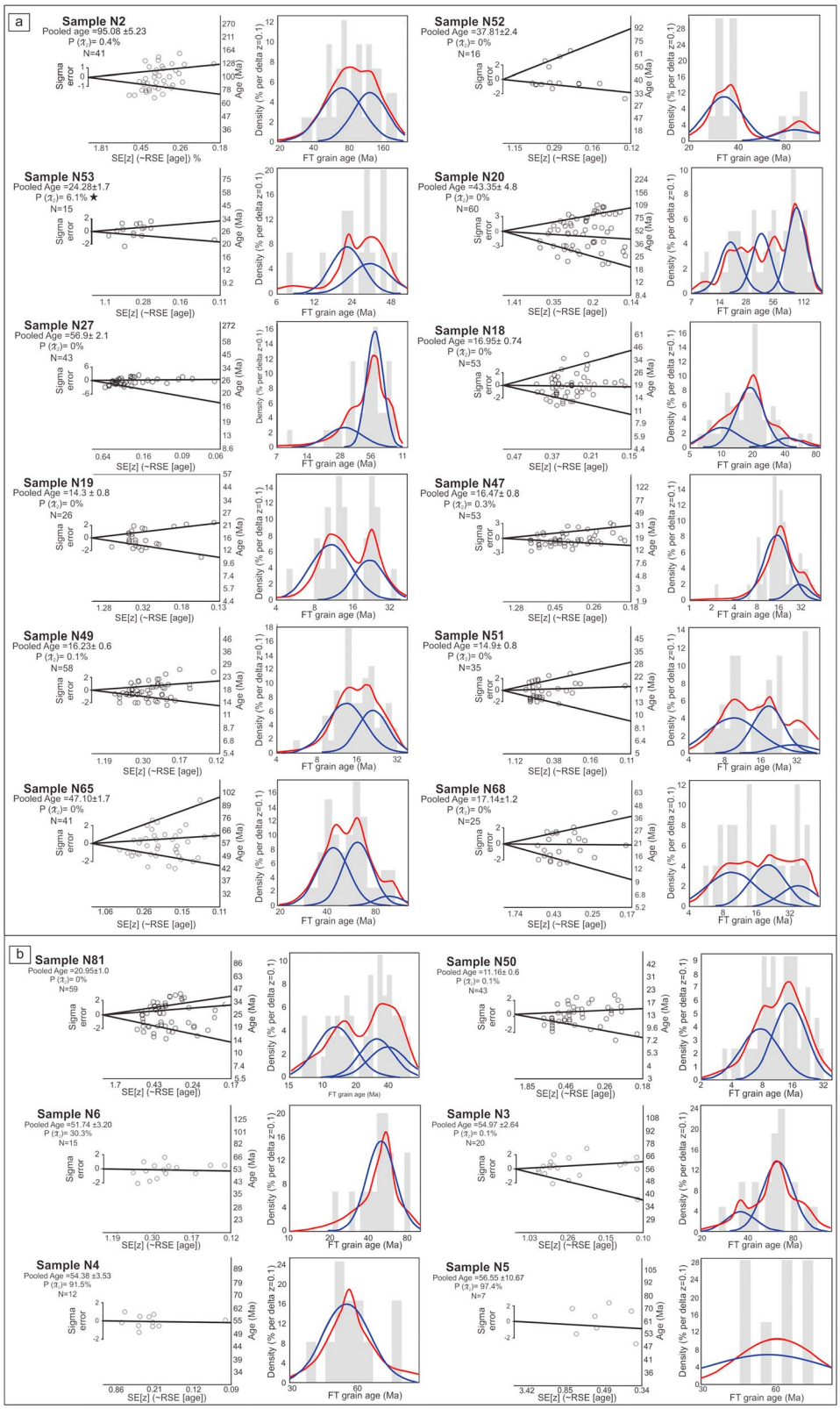

Figure 4. Apatite fission track results. For each sample, the left column is a radial plot of the single-grain age data and the right column is the probability density plots of fission track grain age distributions (Brandon, 1996, 2002). Red lines indicate probability density distributions, and blue lines indicate component distributions estimated by the binomial peak-fit method (Galbraith & Green, 1990).

Table 3
Zircon (U-Th)/He Data

Samples	He (pmol)	U (ng)	Th (ng)	Th/U	Rs (μm)	Raw age	Age error (1σ) (Ma)	Ft	Corrected age (Ma)	Mean age (Ma)
zN32014-1	7.474.092	0.3098	0.1971	0.64	68.52	38.79	3.28	0.71	54.7	66.0 ± 6.1
zN32014-3	12.673.850	0.4070	0.3311	0.81	64.72	48.27	4.07	0.71	67.9	
zN32014-4	279.055.626	0.5445	0.5149	0.94	75.78	77.22	6.19	0.75	103.2	
zN32014-5	42.118.095	12.129	0.9595	0.79	68.66	54.04	4.52	0.72	75.4	
zN42014-1	9.057.806	0.2902	0.2890	1.00	69.4	46.68	3.79	0.74	63.2	69.9 ± 4.4
zN42014-2	25.424.267	0.6856	0.3944	0.58	74.12	60.28	4.85	0.74	80.9	
zN42014-3	14.195.800	0.3733	0.4725	1.27	76.13	54.07	4.40	0.74	73.3	
zN42014-4	3.074.303	0.1166	0.0623	0.53	64.16	43.24	3.74	0.69	62.3	
zN52014-1	22.918.136	0.6796	0.6998	1.03	88.92	50.12	3.87	0.78	64.5	72.2 ± 2.8
zN52014-3	89.859.451	23.795	20.114	0.85	91.13	58.13	4.38	0.80	73.0	
zN52014-4	20.002.231	0.5542	0.5697	1.03	71.12	53.64	4.39	0.73	73.2	
zN52014-5	36.916.470	0.8629	11.501	1.33	86.22	60.07	4.69	0.77	78.1	
zN62014-2	83.305.462	16.040	12.422	0.77	102.38	80.89	6.01	0.81	100.1	93.3 ± 3.9
zN62014-3	84.362.063	17.680	13.268	0.75	80.21	74.74	5.83	0.77	97.1	
zN62014-4	27.393.220	0.6354	0.3659	0.58	74.96	69.99	5.62	0.75	93.6	
zN62014-5	83.404.714	22.460	0.9551	0.43	74.06	62.30	4.94	0.76	82.3	

Note. Ft is the alpha ejection correction factor (Farley, 2002; Farley et al., 1996). Numbers in italic indicate outliers that were discarded before mean age calculation. Mean ages are the mean of each selected aliquot, and the age error is the standard deviation between selected aliquots divided by the square root of the number of aliquots.

column (N65, N27, and N20) display mean track lengths of 11.4 ± 1.2, 12.1 ± 1.2, and 10.6 ± 0.4 μm, respectively, suggesting that they have resided for a detectable amount of time in a partial annealing zone, but it is unclear whether thermal annealing took place primarily in the source area and/or during reheating in the sedimentary basin.

4.4. Fission Track Pooled Ages and Age Components

All the detrital apatite fission track pooled ages obtained in the Mesozoic units of the Neuquén Basin are younger than the stratigraphic age of the strata from which they are derived, which means that all the samples have been reset to variable extents. Most FTGA distributions, with the exception of samples N5, N4, and N6, have a wide range of cooling ages such that it is likely that the youngest grains have been selectively reset to form the youngest age components (Garver et al., 1999). This differential behavior may be related in some cases to substitutions in the crystalline lattice, which may contribute to a greater or lesser resistance to the annealing of the tracks in the grains (Green et al., 1989; Ketcham et al., 1999). We unfortunately could not find systematic correlations between the different elemental concentrations in apatite crystals and the peak ages (see S3 section in the supporting information). On the other hand, the location of the samples within the sedimentary column also plays an important role on age correlations, because the deeper the samples were buried, the higher the temperatures were and the more the AFT ages from the source rocks (preexisting rocks) were reset. Down to sample N50, the pooled ages progressively decrease with increasing depth (Tables 2 and

Table 4
Apatite (U-Th)/He Data

Samples	^{238}U (ppm)	^{232}Th (ppm)	^{147}Sm (ppm)	^{4}He (fmol)	Mean L (μm)	Mean R (μm)	Raw age (Ma)	Error (Ma)	Ft	Corrected age	Mean age (Ma)
aN32014–1	1.1	16.4	23.2	0.1	151.59	66.42	2.31	0.24	0.58	4.0	30.3 ± 5.8
aN32014–2	0.8	12.9	16.4	1.0	188.28	71.63	22.75	2.24	0.61	37.3	
aN32014–3	3.5	16.7	30.1	0.8	118.56	59.32	22.42	2.53	0.53	42.2	
aN32014–4	6.6	39.6	39.8	1.0	119.62	60.21	13.32	1.49	0.53	24.9	
aN32014–5	1.8	27.3	19.9	0.5	175.61	59.69	9.30	1.01	0.55	16.9	
aN52014–1	1.5	14.9	20.0	0.8	127.7	89.88	12.86	1.19	0.65	19.8	19.4 ± 2.3
aN52014–2	2.5	20.7	21.3	0.8	125.81	74.91	14.03	1.40	0.60	23.3	
aN52014–3	4.9	37.1	28.1	1.0	113.79	64.61	13.96	1.52	0.55	25.3	
aN52014–4	5.9	55.0	39.8	1.4	157.76	69.87	8.76	0.88	0.60	14.7	
aN52014–5	3.4	78.0	31.1	0.9	119.02	65.47	7.56	0.82	0.56	13.6	

Table 5
Best Fit Age Populations for Apatite FTGA Distributions

Sample	Stratigraphic age (Ma)	N	AFT age range (Ma)	P_1	P_2	P_3	P_4	P_5	P_6
N2	~100–70	41	32.8–199	xxx	xxx	xxx	xxx	71.9 ± 15.7/20.0 56.2%	126.1 ± 26.7/33.7 43.8%
N52	[115–113]	16	27–98.5	xxx	xxx	xxx	32.7 ± 4.4/5.1 77.0%	xxx	91.6 ± 23.2/31.1 23.0%
N53	[133.8–132.5]	15	7.1–48.5	xxx	xxx	21.3 ± 4.5/5.7 55.6%	32.5 ± 9.2/12.9 44.4%	xxx	xxx
N20	[133.8–132.5]	60	8.8–142	xxx	xxx	18.7 ± 3.2/3.9 28.6%	40.8 ± 8.6/10.9 29.7%	xxx	97.7 ± 11.6/11.9 41.7%
N27	[133.8–132.5]	43	7.4–88.9	xxx	xxx	xxx	31.2 ± 6.8/8.7 31.6%	60.7 ± 4.7/7.1 67.1%	xxx
N18	[139.5–137.5]	53	6.1–68.5	9.9 ± 1.4/3.4 26.8%	xxx	18.5 ± 2.5/3.0 63.2%	42.0 ± 11.1/15.1 10.0%	xxx	xxx
N19	[139.5–137.5]	26	3.3–31.5	10.7 ± 1.7/2.1 64.5%	xxx	21.6 ± 3.8/4.6 35.5%	xxx	xxx	xxx
N47	[139.5–137.5]	53	1.5–37.9	xxx	14.4 ± 1.9/2.2 84.9%	xxx	28.6 ± 7.7/10.6 15.1%	xxx	xxx
N49	[139.5–137.5]	58	5–30	xxx	13.2 ± 1.8/2.1 61.5%	21.3 ± 3.1/3.7 38.5%	xxx	xxx	xxx
N51	[139.5–137.5]	35	5.0–36.6	9.4 ± 1.7/2.2 50.4%	xxx	18.3 ± 3.3/4.0 41.7%	29.2 ± 13.5/25.2 3.2%	xxx	xxx
N65	[139.5–137.5]	41	30.1–109.1	xxx	xxx	xxx	44.1 ± 5.4/6.1 46.5%	66.3 ± 8.1/9.3 47.1%	97.4 ± 22.7/29.5 5.9%
N68	[139.5–137.5]	25	4.6–44.9	9.6 ± 3.1/4.6 42.5%	xxx	20.3 ± 6.9/10.6 38.8%	37.7 ± 13.0/19.8 18.7%	xxx	xxx
N81	[139.5–137.5]	59	5.5–57.3	xxx	13.1 ± 2.0/2.3 44.5%	xxx	31.5 ± 16.5/34.6 30.0%	39.9 ± 12.3/17.8 25.5%	xxx
N50	[~157.3–150.0]	43	2.9–28.4	7.7 ± 0.9/1.0 43.6%	15.0 ± 1.4/3.2 56.4%	xxx	xxx	xxx	xxx
N6	[174.1–166.1]	15	21.3–79.5	xxx	xxx	xxx	xxx	51.7 ± 6.2/7.0 100%	xxx
N3	[190.8–182.7]	20	26.1–112.7	xxx	xxx	xxx	36.8 ± 6.7/8.3 21.7%	64.4 ± 6.9/7.7 78.3%	xxx
N4	[190.8–182.7]	12	37.4–91.0	xxx	xxx	xxx	xxx	54.6 ± 6.7/7.7 100%	xxx
N5	[190.8–182.7]	7	45.6–80.4	xxx	xxx	xxx	xxx	56.6 ± 17.5/25.3 100%	xxx

Note. Binomial peak-fit ages (P_1–P_7) were determined using *Binomfit* (Brandon, 1996, 2002) and are indicated by their mean age ± 2 standard errors, their relative abundance (%), and *N* the total number of grains dated.

5 and Figure 5) as does the single-grain age dispersion (Tables 2 and 5) indicating an increasing degree of age resetting toward the base of the stratigraphic section (Table 5 and Figure 5). This is in agreement with vitrinite reflectance data collected by Muñoz (1996) in shales from the Los Molles (Early Jurassic), Vaca Muerta (Late Jurassic-Early Cretaceous), and Agrio (Early Cretaceous) formations (see Tables 2 and S4). This data set indicates that peak burial temperatures increased from 119.5 ± 9.9 to 215.6 ± 9.0 °C between stratigraphic depths of 1,225–3,715 m (Table S4 and Figure S4). Therefore, the samples that were partially reset bear youngest populations P_1 and P_2, in the range of 7.7 ± 0.9/1.0 to 15.0 ± 1.4/3.2 Ma, which we interpret to be the result of middle to late Miocene cooling/exhumation episodes that will be discussed in section 5 in the context of additional geological evidence.

The older age components are, in general, of limited use to our study since they represent inherited source ages that have variably been reset during deposition and subsequent burial in the sedimentary basin. However, despite showing pooled ages in the range of the P_5 population, the four samples located at the base of the basin are of different nature because they pass the χ^2 test (Tables 2 and 5), which means that they have most likely been fully reset and then were cooled from temperatures >120 °C ± 20 °C during a subsequent cooling and exhumational episode. These samples are N4, N5, and N6 with ages ranging from

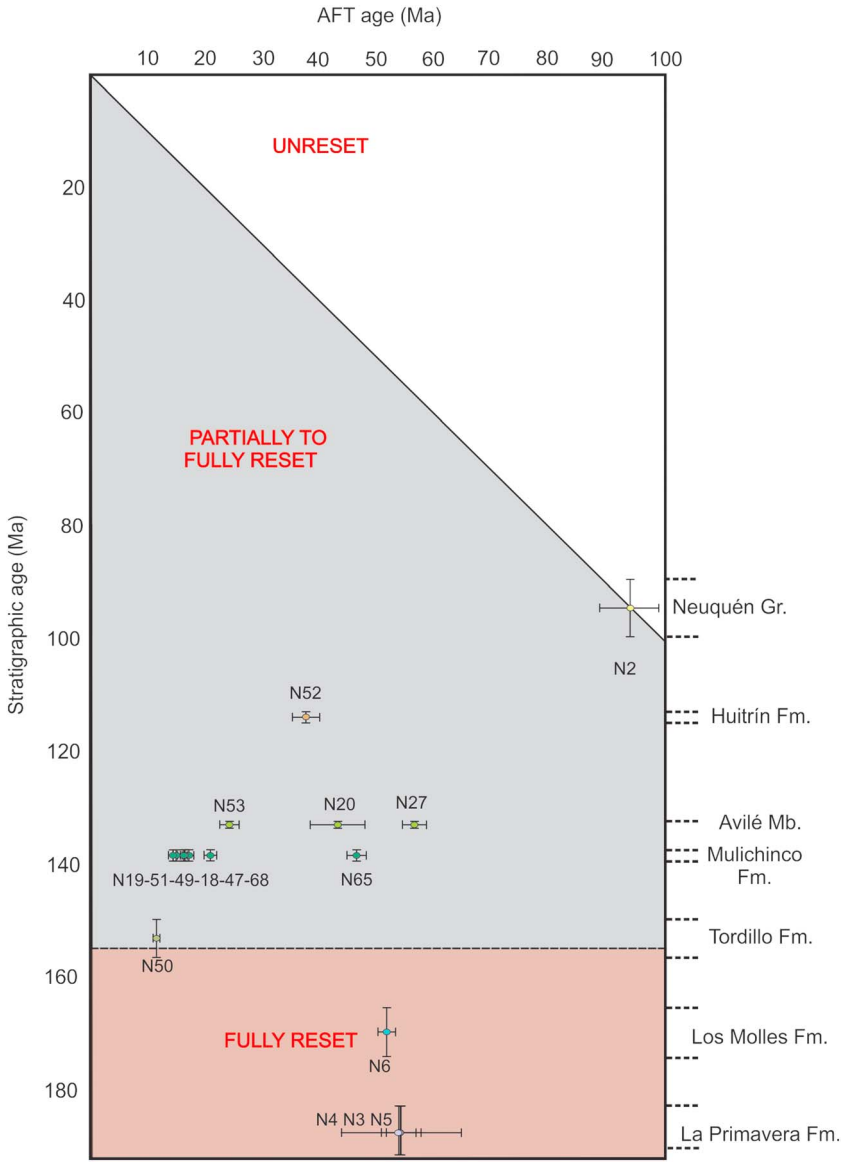

Figure 5. Pooled apatite fission track ages plotted against the stratigraphic age of the sampled formations. All the samples have been reset to various degrees during burial in the sedimentary basin. The grains of the Early-Jurassic La Primavera and Los Molles Formations, the basal units of the stratigraphic pile in this sector of the Neuquén Basin, passed the χ^2 test showing that they were fully reset (Table 2). On the other hand, the Tordillo and Mulichinco Formations display two or more populations (Table 5) formed by grains that have undergone partial annealing and others that are heavily to fully reset. The ages shown correspond to the youngest peak ages obtained using the *Binomfit* program (Brandon, 1996, 2002). Sample N2 was not reset because of the lack of burial.

51.7 ± 3.2 to 56.5 ± 10.7 Ma and sample N3 that shows some single-grain age dispersion (Table 2) yet yields a pooling age of 54.9 ± 2.6 Ma, identical to the aforementioned samples.

4.5. Zircon and Apatite (U-Th)/He Results

The mean ZHe ages range from 93.3 ± 3.9 Ma to 54.7 ± 6.1 Ma (Table 3). In the sample N3, the fourth aliquot produced an age that was significantly older and was removed from the mean ZHe age calculation. The discarded aliquot was fractured and showed minor abrasions on its surface, which could have adversely affected its age. Other factors that could have contributed to this age anomaly include potential zonation of uranium and radiation damage (e.g., Reiners, 2005). The three deepest samples of the section were collected in La Primavera Formation and are, from bottom to top, N5, N4, and N3 (Table 1). We know from our AFT data

a Cooling rates for the Cordillera del Viento

Sample N3	Cooling age (Ma)	Age error (Ma)	Closure temperature (°C)	Error (°C)	Cooling rate (°C/Ma)	Error (°C/Ma)
AHe	30.3	5.8	70	20	**2.0**	**1.3**
AFT	54.9	2.6	120	20		
ZHe	66	6.1	180	20	**5.4**	**4.1**
Sample N4						
AHe	xx	xx	70	20		
AFT	54.4	3.5	120	20		
ZHe	69.9	4.4	180	20	**3.9**	**2.3**
Sample N5						
AHe	19.4	2.3	70	20	**1.3**	**0.9**
AFT	56.5	10.6	120	20		
ZHe	72.2	2.8	180	20	**3.8**	**3.2**

References
A-He age AFT age Zr-He age

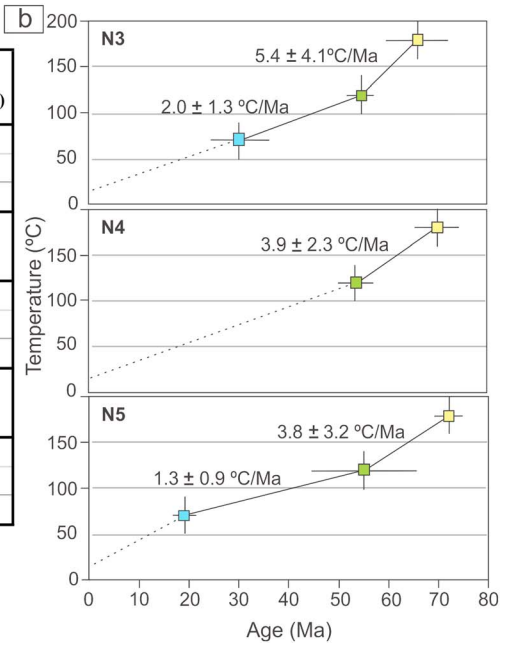

Figure 6. (a) Data used to construct cooling curves and (b) cooling curves calculated from cooling ages and closure temperatures of AFT, AHe, and ZHe thermochronological systems. The errors on cooling ages and closure temperatures were propagated into the error of the cooling rates.

that these have been fully reset at temperatures >120 °C (Figure 5). This is confirmed by a mean random vitrinite reflectance value of 2.70 ± 0.3% R_m for a sample from Los Molles Formation (BRD01-24 in Table 1; Muñoz, 1996), stratigraphically located on top of samples N3–N5. The empirical calibration of R_m by Barker and Pawlewicz (1994) yields a peak temperature of burial, T_{peak} of around 215.6 ± 9.0 °C, which indicates that the ZHe thermochronometer has also been fully reset in these samples (Table S4 and Figure S4).

They show ages ranging from 72.2 ± 2.8 to 66.0 ± 6.1 Ma, which are within errors identical, suggesting that they were cooled below temperatures of 180 ± 20 °C about 70 Ma ago. The sample N6 collected in the overlying Los Molles Formation yields an older age of 93.3 ± 3.9 Ma that could be attributed to an earlier cooling due to its higher position in the stratigraphic column. The two AHe ages obtained from samples N3 and N5 are 30.3 ± 5.8 Ma and 19.4 ± 2.3 Ma, respectively.

4.6. Cooling Rates in the Cordillera del Viento

The three stratigraphically lowermost samples N3-N4-N5 are currently located in the Cordillera del Viento and have been reset at temperature >210 °C. In the absence of measurable confined track lengths, we have chosen to empirically construct cooling curves (Figure 6b). We keep in mind that the cooling ages for ZHe, AFT, and AHe could only be apparent ages due to their relatively slow cooling and hence potential residence in their respective partial retention zones. Hence, the cooling ages and the rates provided hereafter might represent minimum (younger) ages and maximum rates, respectively. With this in mind, we have calculated the cooling rates of samples N3–N5 (Figure 6a) and propagated the errors on ages and closure temperatures to calculate the errors on the cooling rates. The results are remarkably consistent and show that between about 70 and 56 Ma, the Cordillera del Viento was cooled at rates ranging from 5.4 ± 4.1 to 3.8 ± 3.2 °C/Ma. After 51–56 Ma until the present, cooling have very slightly decreased down between 2.1 ± 1.3 and 1.4 ± 0.9 °C/Ma (Figure 6b). This slight deceleration may have a tectonic origin and be due to the cessation of activity of the Andacollo back thrust 56–51 Ma ago (Figure 7). However, within errors, this deceleration is not detectable and cooling rates may only reflect a slow and overall steady cooling of the Cordillera del Viento since 70 Ma.

5. Structural Evolution of the Chos Malal FTB

We propose a new structural evolution of the Chos Malal FTB based on our structural and thermochronological data, and on existing geological data, and qualitatively place it in the context of the critical wedge

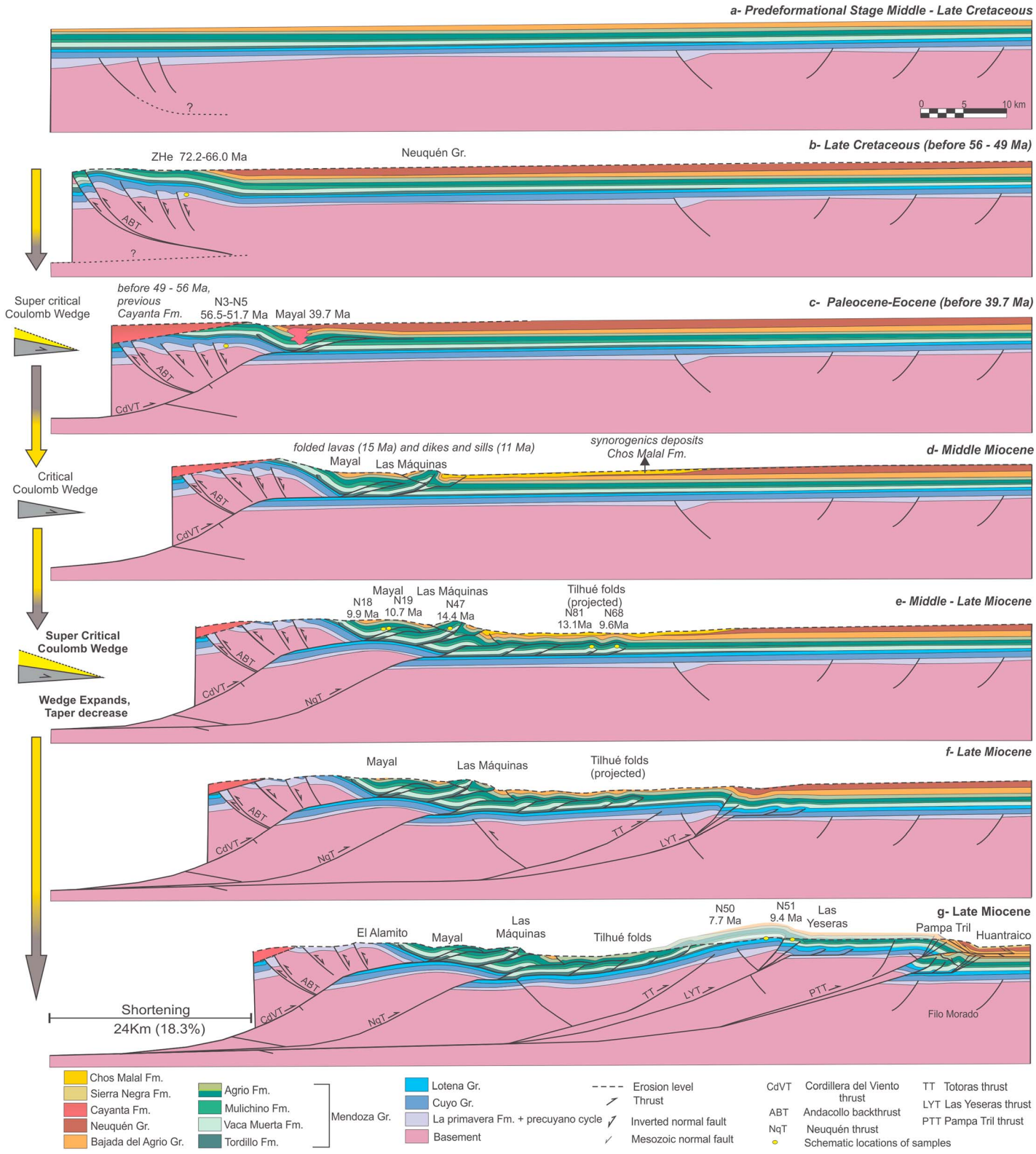

Figure 7. Structural evolution for the Chos Malal FTB. Diagrams on the left side represent the potential state of the Coulomb wedge for the main deformational stages (a) precontractional stage; (b, c) onset of Andean compression during the Late Cretaceous-Paleogene, through faulting and uplift of the Cordillera del Viento; (d, e) related thick- and thin-skinned structures completed the deformation in the inner zone and created syntectonic deposits; and (f, g) contraction progressed toward the foreland through the basement-involved Las Yeseras thrust (LYT) and Pampa Tril thrust (PTT), and the thin-skinned Filo Morado anticline. Out-of-sequence branch of the PTT created a large basement uplift, whose eastward displacement was compensated by back thrusting in a triangle zone.

model (e.g., Davis et al., 1983). This model explains the development of orogenic wedges considering the critical taper between the basal décollement and the surface slope. The shape of an orogenic wedge is controlled by the basal friction, the strength of the material, and erosion Buiter, 2012). The taper angle is referred to a critical value, dependent on the coefficient of friction at the base of the wedge and the strength of the rocks that compose it. When the taper angle is below that value, the wedge is subcritical and deforms internally to increase the taper, until the critical shape is reached. If the critical wedge is forced to accrete new material (e.g., by syntectonic sedimentation), it will continuously deform to maintain its critical taper (Dahlen & Suppe, 1988; Davis et al., 1983). Changes in the critical taper promote the alternate growth of new structures in both the internal and external zones of the wedge; thus, we consider qualitatively these mechanisms in order to explain the structural development of the Chos Malal FTB.

5.1. Late Cretaceous-Paleogene Deformation in the Chos Malal FTB

The pre-Andean Paleozoic basement was affected by normal faults and covered by synrift deposits themselves sealed by Jurassic and Cretaceous postrift sedimentary units (Figures 3c and 7a; Gulisano et al., 1984; Vergani et al., 1995). According to Tunik et al. (2010) and Di Giulio et al. (2012), Andean contractional deformation started 100–88 Ma ago in our study area based on U-Pb dating of detrital zircon from Cretaceous synorogenic units. In our model this early deformation could be associated with the uplift of the western flank of the Cordillera del Viento, in the inner zone of Chos Malal FTB, through the inversion of preexisting eastward dipping normal faults and then by the nucleation and activation of the Andacollo back thrusts system (ABT, Figure 7b). Significant displacement along these structures is required to account for the minimum rock uplift of ~6 km that has generated the observed angular unconformity between the Paleogene volcanics and the Paleozoic basement (Kozlowski et al., 1996, 1998). This deformation must have occurred before 56 Ma, the time at which the Paleogene volcanics were emplaced as indicated by ^{40}Ar-^{39}Ar dating on hornblende (Jordan et al., 2001). Our ZHe and AFT ages from samples N3–N5, ranging from 72.2 ± 2.8 to 66.0 ± 6.1 Ma, and 51.7 ± 3.2 and 56.5 ± 10.7 Ma, respectively, are in agreement with ongoing tectonically driven exhumation of the Cordillera del Viento in the latest Cretaceous-early Paleogene.

The Andacollo west vergent structures created prominent structural relief on the western slope of the Cordillera del Viento, which led the wedge to become super critical and hence triggered the formation of a new major fault, the Cordillera del Viento thrust (CdVT), which propagated eastward (Figure 7c). The basement-involved CdVT flattens upward within the evaporites of the Auquilco Formation and, through a fault-bend folding mechanism, produces wedge geometry on the eastern flank of the Cordillera del Viento (Figure 7c). The eastward displacement of this basement wedge forms second-order structures such as the Sierra del Mayal folds (c in Figure 2a). Importantly, the subvolcanic rocks forming the Sierra del Mayal, which crosscut these folds, were dated at 39.7 ± 0.2 Ma by ^{39}Ar-^{40}Ar on whole rock (Cobbold & Rossello, 2003), which indicates that this folding has occurred before the late Eocene (Figure 7c). Between 70 and 40 Ma, we estimate that one third (~8 km) of horizontal shortening has occurred (Figures 7b and 7c) yielding a shortening rate of 0.26 mm/yr. This number is to be taken with caution because (1) the ABT driving the shortening is not exposed at the surface and its geometry at depth is poorly constrained and (2) the time interval of its activity remains imprecisely constrained.

5.2. Neogene Deformation of the Chos Malal FTB

Contractional deformation during the middle Miocene was restricted to the inner sector of the FTB, which permitted displacement on the CdVT, generating new thin-skinned structures involving the entire Mendoza Group, such as the Las Máquinas anticline (Figure 7d). North of the study area, volcanic rocks dated by ^{40}Ar-^{39}Ar on amphibole and plagioclase at 14.51 ± 0.12 Ma and 14.8 ± 8.0 Ma, respectively (Spagnuolo et al., 2012), are folded (Folguera et al., 2007); further, the emplacement in the Las Máquinas anticline of the Cerro Negro andesitic complex (Figure 1b), dated by U-Pb on zircons at 11.63 ± 0.20 Ma and 11.55 ± 0.06 Ma (Gürer et al., 2016), brackets this first Neogene contractional deformation between 15 Ma and 11 Ma. In our sample N47, from the Las Máquinas anticline, the youngest AFT peak yielded an age of 14.4 ± 1.9/2.2 Ma (Figure 2a and Table 5), which would belong to this middle Miocene stage of deformation. The growth of these structures likely led the orogenic wedge to approach a critical taper geometry, and thus, further deformation continued in normal sequence toward the foreland.

The basement-involved Neuquén thrust (NqT) produced a second basement wedge in front of which the Tilhué fault-related folds were formed (Figure 7e). AFT results of partially annealed samples N68 and N81 collected from the Mulichinco Formation in the Loma Tilhué anticlines and N49 from the Chacayco anticline yielded youngest peak ages at 9.6 ± 3.1/4.6, 13.1 ± 2.0/2.3, and 13.2 ± 1.8/2.1 Ma, respectively (Figures 1b and 2a and Table 5). These ages are similar, within error, to the youngest AFT peaks obtained from samples N19 and N18 located to the west of the Mayal syncline, which display ages of 10.7 ± 1.7/2.1 and 9.9 ± 1.4/3.4 Ma (Figure 2a and Table 5). Some of these samples are now located in the hanging wall of the NqT. There is a high probability that these age components have been fully reset during burial because of their consistency and the high percentage of the total fraction per sample they represent (see Table 5). On samples located in our study area, Muñoz (1996) has used vitrinite reflectance data, an independent thermometric proxy, to suggest that all pre-Mulichinco Formation rock samples have been subjected to paleotemperatures >120 °C that were sufficient to fully anneal predepositional fission tracks. Our AFT data are in relatively good agreement with these findings since the samples located below the Mulichinco Formation have been fully reset except for sample N50 in the Tordillo Formation (Tables 2 and 5). Accordingly, the younger age peaks from Mulichinco Formation (N18 to N81 in Tables 2 and 5) suggest that the cooling below the AFT effective closure temperature may have occurred in response to significant displacement on the NqT between about 13 and 10 Ma (Figure 7e).

At the end of this middle-late Miocene deformation, a large structural relief was likely achieved in the inner zone of the Chos Malal FTB, pushing the orogenic wedge into a super critical state (Figure 7e). In order to return to its critical state, the wedge propagated toward the foreland, creating new thick-skinned structures (Figures 7f). New basement-involved thrusts include the Totoras (TT), the Las Yeseras (LYT), and the Pampa Tril thrusts (PTT), which in turn create complex thin-skinned deformation at the mountain front (Figures 7f). The TT shows significant displacement north of the study transect (Galland et al., 2007) but remains blind with limited displacement within our cross section. Displacement on an upper branch of the LYT has propagated toward the surface, folding the overlying strata forming the Las Yeseras anticline (Figure 7f). The PTT was formed following a normal sequence of forelandward fault propagation and might have triggered the formation of the Filo Morado anticline (Figure 7f), a thin-skinned fold that constitutes one of the most important oil field in the fold-and-thrust belt of the Neuquén Basin (Selva et al., 2005; Zapata et al., 2001). In a second step, an out-of-sequence reverse fault formed in the hanging wall of the PTT, generating significant structural relief (Figure 7f). Eastward displacement of this basement slice is compensated by back thrusting along evaporitic horizons of the Bajada del Agrio Group defining a triangle zone (Figure 7f; Ploszkiewicz & Viñes, 1987; Turienzo et al., 2015, 2018).

The grains of samples N52 and N53 from the Huitrín Formation and the Avilé Member, respectively, located in the Pampa Tril anticline (Figures 1b, 2a, and 7f) were only partially reset, and thus, detrital AFT ages from these samples are of limited use to bring chronologic constraints on the timing of deformation in this area. On the other hand, samples N50 (Tordillo Formation) and N51 (Mulichinco Formation), collected in the flanks of the Las Yeseras anticline (Figure 7f), show much younger AFT peak ages of 7.7 ± 0.9/1 and 9.4 ± 1.7/2.2 Ma (Table 5). These ages represent a fraction of the grains that have been heavily to fully annealed in the sedimentary basin and then cooled through the AFT effective closure temperature sometimes during/after 7–9 Ma. Although it remains challenging to distinguish if this cooling stage is related to the formation of the Las Yeseras structure itself or to that of the Pampa Tril structure, we contend that these ages are a thermal response to the tectonic processes driving the deformation of the outer sector of the Chos Malal FTB during/after 7–9 Ma. The surface uplift of the Pampa Tril anticline at the mountain front has modified the regional slope and consequently might also have pushed the equilibrium of the orogenic wedge toward a subcritical state (Figure 7f). Younger deformation in the hinterland is required for the taper to recover its critical state. Evidences of neotectonic contractional deformation were recognized in the Cura Mallín Basin, to the west of the Cordillera del Viento (Figure 1a), where thrusts and folds affect Quaternary volcanic and sedimentary rocks (Folguera et al., 2007; Sagripanti et al., 2018).

Sequential restoration of our structural cross section shows that about two thirds of horizontal shortening (~16 km) has occurred between 15 and 7 Ma (Figures 7d–7f) yielding shortening rates of 2 mm/yr and suggesting that most of the structural development of the Chos Malal FTB has occurred during the Neogene and, to a lesser extent, might have lasted until the present (Figure 7g).

6. Discussion: Andean Tectonic Development of the Northwestern Part of the Neuquén Basin

Several authors propose that the Andes of the Neuquén province have experienced multiple tectonic stages as a consequence of the change of the plate tectonic boundary configurations (Folguera et al., 2006; Ramos et al., 2014; Ramos & Folguera, 2005; Zapata & Folguera, 2005). The first deformation stage took place during the uppermost Cretaceous (Figures 7a and 7b) due to the shallowing of the subducting plate, as is recorded by the eastward migration of the volcanic arc (Kay et al., 2006; Ramos & Folguera, 2005). Late Cretaceous Neuquén Group was likely deposited as the synorogenic response to the early stages of fold-and-thrust belt development (Cobbold & Rossello, 2003; Di Giulio et al., 2012; Ramos & Folguera, 2005; Rojas Vera et al., 2015; Tunik et al., 2010). Recently, the presence of growth strata into the Neuquén Group was documented in the south of the Mendoza Province (Fennell et al., 2015). To the south of Chos Malal, outside of the study transect, the Neuquén Group overlies the Early Cretaceous Rayoso Formation along an angular unconformity (Leanza, 2009; Ramos & Folguera, 2005; Tunik et al., 2010). U-Pb dating of detrital zircon from Cretaceous units suggests changes in the provenance from foreland-derived (east) zircon for the Rayoso Formation to volcanic arc-derived (west) zircon in the overlying Candeleros Formation at the base of Neuquén Group (Di Giulio et al., 2012; Tunik et al., 2010). This change has been attributed to a shift in the tectonic regime in response to the onset of Andean contraction in the Upper Cretaceous, between 100 and 88 Ma (Di Giulio et al., 2012; Tunik et al., 2010).

West of the Cordillera del Viento, the Paleogene extrusive rocks of the Cayanta Formation (Jordan et al., 2001; Llambías & Rapela, 1987; Zamora Valcarce et al., 2006) rest in angular unconformity on top of rocks of the Andacollo (Carboniferous) and Choiyoi (Permian) Groups (Llambías & Rapela, 1987; Rovere, 1998; Figure 7 c). The crystallization ages of these volcanic rocks have been dated at 56.0 ± 1.1 to 48.9 ± 2.7 Ma using ^{40}Ar-^{39}Ar on hornblende and zircon fission tracks, respectively (Jordan et al., 2001). These ages indicate that significant contraction preceded eruption of the Cayanta Formation. Furthermore, the intrusion of subvolcanic bodies exposed in the Sierra del Mayal, dated with ^{39}Ar-^{40}Ar on whole rock, yielded an age of 39.7 ± 0.2 Ma (Cobbold & Rossello, 2003; Figures 2 and 7c) and in the Cerro Caycayén an age of 44.7 ± 2.2 Ma, using K-Ar in amphibole, (Llambías & Rapela, 1989). These subvolcanic bodies are emplaced after this stage of deformation and crosscut or offset the axial planes of the folds in the Mendoza Group (Cobbold & Rossello, 2003; Sánchez et al., 2015). It is worth noting that a previous study involving inverse modeling of AFT data suggested the occurrence of a significant exhumation stage between 70 and 40 Ma (Rojas Vera et al., 2015) Our multithermochronometric data set suggests that cooling of the Cordillera del Viento, in the inner zone of the Chos Malal FTB, started at least 70 Ma ago in agreement with most of the previous data. Cooling rates from the Cordillera del Viento range from 5.4 ± 4.1 to 3.8 ± 3.2 °C/Ma between 70 and 55 Ma and are probably related to the activity of the Andacollo back thrusts (Figures 6 and 7b). The Cura Mallín Basin, located in the hinterland between the current Andean volcanic arc in the west and the Cordillera del Viento in the east (Figure 1), is a target to constrain post-Eocene deformation regimes because it has preserved Oligocene-early Miocene volcaniclastic deposits. However, there are many disagreements as to its origin. Some authors interpret these deposits as resulting from extensional deformation affecting the retroarc zone and interrupting Andean contraction (Burns et al., 2006; Folguera et al., 2007; Kay et al., 2006; Rojas Vera et al., 2015), while others argue that the Cura Mallín Basin is a compressional foreland basin (Cobbold et al., 2008; Cobbold & Rossello, 2003; Lesta et al., 1985), others an intra-arc basin (Burns et al., 2006; Jordan et al., 2001; Melnick et al., 2006; Muñoz et al., 2000; Radic, 2010; Radic et al., 2002; Suárez & Emparán, 1995), and others that it is a pull-apart-type basin (Godoy et al., 1999; Kay & Mpodozis, 2002; Spalletti & Dalla Salda, 1996; Suárez & Emparán, 1995). AHe cooling ages from early Jurassic rocks in the Cordillera del Viento range from 30.3 ± 5.8 to 19.4 ± 2.3 Ma, indicating an ongoing cooling during the late Oligocene and the early Miocene (Figure 6b). More geological evidence is required in order to demonstrate if such cooling is related to extensional or contractional tectonic. Evidence of the Neogene contractional stage has been recorded along the fold-and-thrust belt. To the northeast of the Cordillera del Viento, lavas and ignimbrites of the Charilehue Formation dated by ^{40}Ar-^{39}Ar on amphibole and plagioclase at 14.51 ± 0.12 Ma and 14.8 ± 8.0, respectively (Spagnuolo et al., 2012), are folded and overthrust by Cretaceous deposits (Folguera et al., 2007). About 8–10 km north of our study area, the Cerro Negro intrusive complex, which consists of sills and N-S striking dikes, was emplaced along the hinge zone of a large, thin-skinned anticline. This intrusive complex dated by U-Pb on zircons at 11.63 ± 0.20 Ma and 11.55 ± 0.06 Ma

is interpreted to have formed synchronously with the tectonic development of the Chos Malal FTB (Gürer et al., 2016). Burns et al. (2006) obtained $^{40}Ar/^{39}Ar$ biotite age of 11.7 ± 0.3 Ma from an ash flow deposit in the Cura Mallin Basin, offset by a reverse fault and an AFT cooling age of 8.9 ± 1.3 Ma for a granitic pluton exposed in the hanging wall of the same reverse fault, which they interpret as the result of thrust-sense displacement on that fault. Back-arc volcanic successions of the Sierra Negra Formation exposed in the Huantraico syncline, dated at 17–19.8 Ma with ^{40}Ar-^{39}Ar using hornblende and whole rock (Dyhr et al., 2013; Kay & Copeland, 2006), are folded at the front of the Chos Malal FTB and indicate that deformation occurred after their emplacement. Most of the previous tectonic studies in the northern Neuquén Andes consider that the last stage of Andean contraction ended in the late Miocene and after that, which the FTB remained undeformed and eroded passively (Ramos & Folguera, 2005; Zamora Valcarce et al., 2009; Zapata & Folguera, 2005). More specifically in the Chos Malal FTB, the few geochronological data available have led some authors to extend Neogene contraction up until ~10 Ma (Folguera et al., 2007; Gürer et al., 2016). AFT data suggest middle Miocene (10–15 Ma) cooling in the inner zone and post 9–7 Ma cooling in the outer zone of the Chos Malal FTB that we associate with ongoing contractional deformation at these time intervals in these different sectors.

7. Conclusions

Detailed field mapping and structural analysis combined with 18 AFT, 4 ZHe, and 2 AHe new data constrain the chronology of the Late Cretaceous-Paleogene and Neogene structural development of the Chos Malal FTB and allow us to draw the following conclusions:

1. Thermochronometric ages vary along the studied transect and spatially coincide with major thick-skinned thrust faults, indicating that cooling events were most likely induced by tectonic processes.
2. In the inner zone, cooling of the Cordillera del Viento started at least 70 Ma ago. Cooling rates from the Cordillera del Viento range from 5.4 ± 4.1 to 3.8 ± 3.2 °C/Ma between 70 and 55 Ma and decrease down to between 2.0 ± 1.3 and 1.3 ± 0.9 °C/Ma after that. This slight deceleration might be due to the cessation of activity of the Andacollo back thrust 55–51 Ma ago.
3. Middle-late Miocene contractional deformation in both the inner and outer sectors of the FTB is clearly documented at ~15–7 Ma, based on the consistent detrital AFT youngest peak ages obtained for nine samples collected in the Oxfordian-Kimmeridgian Tordillo Formation to the Valanginian Mulichinco Formation and distributed along the FTB.
4. The exhumation of the Las Yeseras-Pampa Tril basement-involved anticlines at the mountain front at ~9–7 Ma, slightly younger than previously assumed, suggests a normal sequence of deformation propagation toward the foreland.
5. The total amount of horizontal shortening obtained from cross-section balancing is 23.9 km, which corresponds to 18.2% of the total initial length of the transect. The sequential reconstruction of the thick- and thin-skinned structures of the Chos Malal FTB shows that most of this shortening was achieved during middle-late Miocene.
6. Our study provides constraints on the thermotectonic evolution of the FTB and should help guide and improve the efficiency of oil and gas exploration activities along the Andean thrust front of the Neuquén Basin in the future.

Acknowledgments
The study was funded by CONICET PUE0047CO, PIP 0583, and ANPCyTFONCyT PICT 2015-0419 awarded to L. Dimieri and by an Emerging Leaders of the America Program scholarship from the Department of Foreign Affairs, Trade and Development (Global Affairs Canada) awarded to I. Coutand for N. Sanchez. We thank the Editor Nathan Niemi and anonymous reviewers for the insightful comments that allowed to improve the paper. Technical support for AFT sample preparation provided by Ms. Bertha Louis (Dalhousie fission-track laboratory) and (U-Th)/He by M. Roman Kislitsyn (Dalhousie Noble Gas laboratory) are greatly appreciated. We thank D. Grujic for discussions on some data interpretations. We are grateful to the Subsecretaría de Energía, Minería e Hidrocarburos of the Neuquén Province for providing the seismic and well data and with Gonzalo Zamora Valcarce for his advice on AFTA samples collection. The new data sets presented in this manuscript are available in Tables 2–4 in the main text and in the supporting information.

References

Aguirre-Urreta, B., Pazos, P., Lazo, D., Fanning, M., & Litvak, V. (2008). First U/Pb SHRIMP age of the Hauterivian stage, Neuquén Basin, Argentina. *Journal of South American Earth Sciences*, *26*(1), 91–99. https://doi.org/10.1016/j.jsames.2008.01.001

Allmendinger, R., Zapata, T., Manceda, R., & Dzelalija, F. (2004). Trishear kinematic modeling of structures, with examples from the Neuquén Basin, Argentina. In K. McClay (Ed.), *Thrust Tectonics and Hydrocarbon Systems, AAPG memoir* (Vol. 82, pp. 356–371).

Allmendinger, R. W. (2012). Fault Fold Forward.v.6. Retrieved from http://www.geo.cornell.edu/geology/faculty/RWA/programs/faultfold-forward-v-6.html

Arregui, C., Carbone, O., & Leanza, H. A. (2011). Contexto tectosedimentario. In H. Leanza, et al. (Eds.) (pp. 29–36). Neuquén: Asociación Geológica Argentina.

Barbarand, J., Carter, A., Wood, I., & Hurford, A. J. (2003). Compositional and structural control of fission-track annealing in apatite. *Chemical Geology*, *198*(1-2), 107–137. https://doi.org/10.1016/S0009-2541(02)00424-2

Barker, C. E., & Pawlewicz, M. J. (1994). Calculation of vitrinite reflectance from thermal histories and peak temperatures: A comparison of methods. In P. K. Mukhopadhyay, & W. G. Dow (Eds.), *Vitrinite reflectance as a maturity parameter* (pp. 216–229). Washington, DC: American Chemical Society. https://doi.org/10.1021/bk-1994-0570.ch014

Brandon, M. T. (1992). Decomposition of fission-track grain-age distributions. *American Journal of Science*, *292*(8), 535–564. https://doi.org/10.2475/ajs.292.8.535

Brandon, M. T. (1996). Probability density plots for fission-track age distributions. *Radiation Measurements*, *26*(5), 663–676. https://doi.org/10.1016/S1350-4487(97)82880-6

Brandon, M. T. (2002). Decomposition of mixed grain age distributions using Binomfit. *On Track*, *24*, 13–18.

Buiter, S. J. H. (2012). A review of brittle compressional wedge models. *Tectonophysics*, *530–531*, 1–17. https://doi.org/10.1016/j.tecto.2011.12.018

Burns, W. M., Jordan, T. E., Copeland, P., & Kelley Shari, A. (2006). The case for extensional tectonics in the Oligocene-Miocene Southern Andes as recorded in the Cura Mallín basin (36°–38°S). In S. M. Kay, & V. A. Ramos (Eds.), *Evolution of an Andean Margin: A tectonic and magmatic view from the Andes to the Neuquén Basin (35°–39°S Lat)*. *Geological Society of America, Special Paper, 407*, 163–184.

Carlson, W. D., Donelick, R. A., & Ketcham, R. A. (1999). Variability of apatite fission-track annealing kinetics I: Experimental results. *American Mineralogist*, *84*(9), 1213–1223. https://doi.org/10.2138/am-1999-0901

Charrier, R., Pinto, L., & Rodríguez, M. P. (2007). Tectonostratigraphic evolution of the Andean Orogen in Chile. In T. Moreno, & W. Gibbons (Eds.), *The geology of Chile* (pp. 21–114). London: Geological Society.

Cobbold, P. R., & Rossello, E. A. (2003). Aptian to recent compressional deformation, foothills of the Neuquén Basin, Argentina. *Marine and Petroleum Geology*, *20*(5), 429–443. https://doi.org/10.1016/S0264-8172(03)00077-1

Cobbold, P. R., Rossello, E. A., & Marques, F. O. (2008). Where is the evidence for Oligocene rifting in the Andes? Is it in the Loncopué Basin of Argentina? In International Symposium on Andean Geodynamics, No. 7: 148–151. Niza.

Coutand, I., Barrier, L., Govin, G., Grujic, D., Hoorn, C., Dupont-Nivet, G., & Najman, Y. (2016). Late Miocene-Pleistocene evolution of India-Eurasia convergence partitioning between the Bhutan Himalaya and the Shillong Plateau: New evidences from foreland basin deposits along the Dungsam Chu section, eastern Bhutan. *Tectonics*, *35*, 2963–2994. https://doi.org/10.1002/2016TC004258

Dahlen, F. A., & Suppe, J. (1988). Mechanics, growth, and erosion of mountain belts. In: Clark, S. P. (ed.) processes in continental lithospheric deformation. *Geological Society of America, Special Papers*, *218*, 161–178. https://doi.org/10.1130/SPE218-p161

Dahlstrom, C. D. A. (1969). Balanced cross sections. *Canadian Journal of Earth Sciences*, *6*(4), 743–757. https://doi.org/10.1139/e69-069

Davis, D., Suppe, J., & Dahlen, F. (1983). Mechanics of fold and thrust belts and accretionary wedges. *Journal of Geophysical Research*, *88*, 1153–1172. https://doi.org/10.1029/JB088iB02p01153

Di Giulio, A., Ronchi, A., Sanfilippo, A., Tiepolo, M., Pimentel, M., & Ramos, V. (2012). Detrital zircon provenance from the Neuquén Basin (south-central Andes): Cretaceous geodynamic evolution and sedimentary response in a retroarc foreland basin. *Geology*, *40*(6), 559–562. https://doi.org/10.1130/G33052.1

Donelick, M. B., Ketcham, R. A., & Carlson, W. D. (1999). Variability of apatite fission-track annealing kinetics: II. Crystallographic orientation effects. *American Mineralogist*, *84*(9), 1224–1234. https://doi.org/10.2138/am-1999-0902

Donelick, R. A., O'Sullivan, P. B., & Ketcham, R. A. (2005). Apatite fission-track analysis. *Reviews in Mineralogy and Geochemistry*, *58*(1), 49–94. https://doi.org/10.2138/rmg.2005.58.3

Dyhr, C. T., Holm, P. M., Llambías, E. J., & Scherstén, A. (2013). Subduction controls on Miocene back-arc lavas from Sierra de Huantraico and La Matancilla, Argentina and new $^{40}Ar/^{39}Ar$ dating from the Mendoza region, Argentina. *Lithos*, *179*, 67–83. https://doi.org/10.1016/j.lithos.2013.08.007

Erslev, E. A. (1991). Trishear fault-propagation folding. *Geology*, *19*(6), 617–620. https://doi.org/10.1130/0091-7613(1991)019%3C0617:TFPF%3E2.3.CO;2

Farley, K. A. (2002). (U-Th)/He dating: Techniques, calibrations, and applications. *Reviews in Mineralogy and Geochemistry*, *47*(1), 819–844. https://doi.org/10.2138/rmg.2002.47.18

Farley, K. A., Wolf, R. A., & Silver, L. T. (1996). The effects of long alpha-stopping distances on (U-Th)/He ages. *Geochimica et Cosmochimica Acta*, *60*(21), 4,223–4,229. https://doi.org/10.1016/S0016-7037(96)00193-7

Fennell, L. M., Folguera, A., Naipauer, M., Gianni, G., Rojas Vera, E., Bottesi, G., & Ramos, V. A. (2015). Cretaceous deformation of the southern Central Andes: Synorogenic growth strata in the Neuquen Group (35°30′-37°S). *Basin Research*, *29*(1), 51–72.

Fleischer, R. L., Price, P. B., & Walker, R. M. (1975). *Nuclear tracks in solids: Principles and techniques* (605 pp.). Berkeley: University of California Press.

Folguera, A., Bottesi, G., Duddy, I., Martín-González, F., Orts, D., Sagripanti, L., et al. (2015). Exhumation of the Neuquén Basin in the southern Central Andes (Malargüe fold and thrust belt) from field data and low-temperature thermochronology. *Journal of South American Earth Sciences*, *64*, 381–398. https://doi.org/10.1016/j.jsames. 2015.08.003

Folguera, A., Bottesi, G., Zapata, T. R., & Ramos, V. A. (2008). Crustal collapse in the Andean back-arc since 2 Ma: Tromen volcanic plateau, Southern Central Andes (36°40′-37°30′S). *Tectonophysics*, *459*, 140–160.

Folguera, A., Ramos, V., Zapata, T., & Spagnuolo, M. (2007). Andean evolution at the Guañacos and Chos Malal fold and thrust belts (36°30′-37°S). *Journal of Geodynamics*, *44*(3-5), 129–148. https://doi.org/10.1016/j.jog.2007.02.003

Folguera, A., Ramos, V. A., González Díaz, E., & Hermanns, R. (2006). Miocene to Quaternary deformation of the Guañacos fold and thrust belt in the Neuquén Andes between 37° and 37° 30´S. In S. M. Kay, & V. A. Ramos (Eds.), *Evolution of an Andean Marg: A tectonic and magmatic view from the Andes to the Neuquén Basin (35° -3 9° S latitude)*. *Geological Society of America, Special Paper, 407*, 247–266.

Franchini, M., López-Escobar, L., Schalamuk, I. B., & Meinert, L. (2003). Magmatic characteristics of the Paleozoic Cerro Nevazón region and other Late Cretaceous and Early Terciary calc-alcaline subvolcanic and plutonic units in the Neuquén Andes, Argentina. *Journal of South American Earth Sciences*, *16*, 399–421.

Franzese, J. R., Spalletti, L. A., Gómez Pérez, I., & Macdonald, D. (2003). Tectonic and paleoenviromental evolution of Mesozoic sedimentary basins along the Andean foothills of Argentina (32°-54°S). *Journal of South American Earth Sciences*, *16*(1), 81–90. https://doi.org/10.1016/S0895-9811(03)00020-8

Galbraith, R. F. (1981). On statistical models for fission track counts. *Mathematical Geology*, *13*(6), 471–478. https://doi.org/10.1007/BF01034498

Galbraith, R. F., & Green, P. F. (1990). Estimating the component ages in a finite mixture. *Nuclear Tracks and Radiation Measurements*, *17*(3), 197–206. https://doi.org/10.1016/1359-0189(90)90035-V

Galland, O., Hallot, E., Cobbold, P., Ruffet, G., & de Bremondd'Ars, J. (2007). Volcanism in a compressional Andean setting: A structural and geochronological study of Tromen volcano (Neuquén province, Argentina). *Tectonics*, *26*, TC4010. https://doi.org/10.1029/2006TC002011

Garrido, A., Kramarz, A., Forasiepi, A., & Bond, M. (2012). Estratigrafía, mamíferos fósiles y edad de las secuencias volcanosedimentarias eoceno-miocenas de la sierra de Huantraico sierra Negra y cerro Villegas (provincia del Neuquén, Argentina). *Andean Geology*, *39*, 482–510.

Garver, J. I., Brandon, M. T., Roden-Tice, M., & Kamp, P. J. J. (1999). Exhumation history of orogenic highlands determined by detrital fission-track thermochronology. In exhumation processes: Normal faulting, ductile flow and erosion (Ed. by U. Ring, M. T. Brandon, G. S. Lister andS.D. Willett). *Geological Society of London*, *154*(1), 283–304. https://doi.org/10.1144/GSL.SP.1999.154.01.13

Gleadow, A. J. W., & Duddy, I. R. (1981). A natural long-term annealing experiment for apatite. *Nuclear Tracks*, *5*(1-2), 169–174. https://doi.org/10.1016/0191-278X(81)90039-1

Godoy, E., Yañez, G., & Vera, E. (1999). Inversion of an Oligocene volcanotectonic basin and uplifting of its superimposed Miocene magmatic arc in the Chilean Central Andes: First seismic and gravity evidences. *Tectonophysics*, *306*(2), 217–236. https://doi.org/10.1016/S0040-1951(99)00046-3

Green, P. F. (1981). A new look at statistics in fission track dating. *Nuclear Tracks and Radiation Measurements*, *5*(1-2), 77–86. https://doi.org/10.1016/0191-278X(81)90029-9

Green, P. F., Duddy, I. R., Gleadow, A. J. W., & Tingate, P. R. (1985). Fission track annealing in apatite: Track length measurements and the form of the Arrhenius plot. *Nuclear Tracks and Radiation Measurements*, *10*(3), 323–328. https://doi.org/10.1016/0735-245X(85)90121-8

Green, P. F., Duddy, I. R., Gleadow, A. J. W., Tingate, P. R., & Laslett, G. M. (1986). Thermal annealing of fission tracks in apatite: 1. A qualitative description. *Chemical Geology*, *59*, 237–253. https://doi.org/10.1016/0168-9622(86)90074-6

Green, P. F., Duddy, I. R., Laslett, G. M., Hegarty, K. A., Gleadow, A. J. W., & Lovering, J. F. (1989). Thermal annealing of fission tracks in apatite 4, quantitative modeling techniques and extension to geological time scales. *Chemical Geology (Isotope Geoscience Section)*, *79*(2), 155–182. https://doi.org/10.1016/0168-9622(89)90018-3

Gulisano, C. A., & Gutiérrez Pleimling, A. R. (1995). The Jurassic of Neuquén Basin: A Neuquén Province, Field Guide, Secretaría de Minería de la Nación y Asociación Geológica Argentina, Serie E, 2, 111 pp., Buenos Aires.

Gulisano, C. A., Gutiérrez Pleimling, A. R., & Digregorio, R. E. (1984). Esquema estratigráfico de la secuencia jurásica del oeste de la provincia del Neuquén, 9° Congreso Geológico Argentino, San Carlos de Bariloche. *Actas*, *1*, 236–259.

Gürer, D., Galland, O., Corfu, F., Leanza, H., & Sassier, C. (2016). Structure and evolution of volcanic plumbing systems in fold-and-thrust belts: A case study of the Cerro Negro de Tricao Malal, Neuquén Province, Argentina. *Geological Society of America Bulletin*, *128*(1–2), B31341.1–B31341.331. https://doi.org/10.1130/B31341.1

Hurley, P. M., & Goodman, C. (1941). Helium retention in common rock minerals. *Bulletin Geological Society of America*, *52*(4), 545–559. https://doi.org/10.1130/GSAB-52-545

Jordan, T., Burns, W., & Veiga, R. (2001). Extension and basin formation in the southern Andes caused by increased convergence rate: A mid-Cenozoic trigger for the Andes. *Tectonics*, *20*, 308–324. https://doi.org/10.1029/1999TC001181

Kay, S. M., Burns, M., & Copeland, P. (2006). Upper Cretaceous to Holocene magmatism and evidence for transient Miocene shallowing of the Andean subduction zone under the northern Neuquén Basin. In S. M. Kay, & V. A. Ramos (Eds.), *Evolution of an Andean margin: A tectonic and magmatic view from the Andes to the Neuquén Basin (35–39°S). Geological Society of America, Special Paper, 407*, 19–60.

Kay, S. M., & Copeland, P. C. (2006). Early to middle Miocene backarc magmas of the Neuquén Basin: Geochemical consequences of the slab shallowing and the westward drift of South America. In S. M. Kay, & V. A. Ramos (Eds.), *Evolution of an Andean Margin: A tectonic and magmatic view from the Andes to the Neuquén Basin (35°-39°S lat). Geological Society of America, Special Paper, 407*, 215–246. https://doi.org/10.1130/2006.2407

Kay, S. M., & Mpodozis, C. (2002). Magmatism as a probe to the Neogene shallowing of the Nazca plate beneath the modern Chilean flat-slab. *Journal of South American Earth Sciences*, *15*(1), 39–57. https://doi.org/10.1016/S0895-9811 (02)00005-6

Ketcham, R. A., Donelick, R. A., & Carlson, W. D. (1999). Variability of apatite fission-track annealing kinetics: III. Extrapolation to geological time scales. *American Mineralogist*, *84*(9), 1235–1255. https://doi.org/10.2138/am-1999-0903

Kozlowski, E., Cruz, C., & Sylwan, C. (1996). Geología estructural de la zona de Chos Malal, Cuenca Neuquina, Argentina. In *13° Congreso Geológico Argentino and 3° Congreso Argentino de Exploración de Hidrocarburos (Buenos Aires), Actas* (Vol. 1, pp. 15–26).

Kozlowski, E., C. Cruz, & C. Sylwan (1998). Modelo exploratorio en la faja corrida de la Cuenca Neuquina. Argentina, Boletín de Informaciones Petroleras, 4–23, Buenos Aires.

Laslett, G. M., & Galbraith, R. F. (1996). Statistical modelling of thermal annealing of fission tracks in apatite. *Geochimica et Cosmochimica Acta*, *60*(24), 5117–5131. https://doi.org/10.1016/S0016-7037(96)00307-9

Laslett, G. M., Green, P. F., Duddy, I. R., & Gleadow, A. J. W. (1987). Thermal annealing of fission tracks in apatite: 2. A quantitative analysis. *Chemical Geology (Isotope Geoscience Section)*, *65*(1), 1–13. https://doi.org/10.1016/0168-9622(87)90057-1

Leanza, H. (2003). Las sedimentitas huitrinianas y rayosianas (Cretácico inferior) en el ámbito central y meridional de la cuenca Neuquina, Argentina. In *Serie Contribuciones Técnicas-Geología, Servicio Geológico Minero Argentino* (Vol. 2, pp. 1–31). Buenos Aires.

Leanza, H. (2009). Las principales discordancias del Mesozoico de la Cuenca Neuquina según observaciones de superficie. *Revista del Museo Argentino de Ciencias Naturales*, *11*(2), 145–184. https://doi.org/10.22179/REVMACN.11.257

Leanza, H., Mazzini, A., Corfu, F., Llambías, E., Svensen, H., Planke, S., & Galland, O. (2013). The Chachil limestone (Pliensbachian-earliest Toarcian) Neuquén Basin, Argentina: U-Pb age calibration and its significance on the Early Jurassic evolution of southwestern Gondwana. *Journal of South American Earth Sciences*, *42*, 171–185. https://doi.org/10.1016/j.jsames.2012.07.012

Lesta, P. J., J. Digregorio, & M. A. Mozetic (1985). Presente y futuro de la exploración de petróleo en las cuencas subandinas, Argentina. II Simposio Bolivariano, Exploracio'n Petrolera en las Cuencas Subandinasa, Bogotá, Publicaciones, *3*, 1–35.

Llambías, E., Leanza, H., & Carbone, O. (2007). Evolución tectono-magmática durante el Pérmico al Jurásico Temprano en Cordillera del Viento (37°5′S-37°15′S): Nuevas Evidencias geológicas y geoquímicas del inicio de la Cuenca Neuquina. *Revista de la Asociación Geológica Argentina*, *62*(2), 217–235.

Llambías, E., Leanza, H., & Galland, O. (2011). Agrupamiento volcánico Tromen-Tilhue. In H. Leanza, et al. (Eds.), (pp. 627–636). Neuquén: Geología y Recursos Naturales de La Provincia de Neuquén, Asociación Geológica Argentina.

Llambías, E. J., & Rapela, C. W. (1987). Las vulcanitas de Collipilli y sus relaciones con las provincias volcánicas del Terciario inferior de Neuquén-Mendoza y Patagonia, 10° Congreso Geológico Argentino, Actas 4, 249–251, San Miguel de Tucumán.

Llambías, E. J., & Rapela, C. W. (1989). Las vulcanitas de Colipilli, Neuquén, y su relación con otras unidades paleógenas de la Cordillera. *Revista de la Asociación Geológica Argentina*, *44*, 224–236.

Melnick, D., Rosenau, M., Folguera, A., & Echtler, H. (2006). Neogene tectonics of the western flank of the Neuquén Andes, 37°–39°30′S. In S. M. Kay, & V. A. Ramos (Eds.), *Evolution of an Andean Marg: A tectonic and magmatic view from the Andes to the Neuquén Basin (35°–39°S lat). Geological Society of America, Special Paper, 407*, 73–95.

Messager, G., Nivière, B., Martinod, J., Lacan, P., & Xavier, J. P. (2010). Geomorphic evidence for Plio-Quaternary compression in the Andean foothills of the southern Neuquén Basin, Argentina. *Tectonics*, *29*, TC4003. https://doi.org/10.1029/2009TC002609

Mitra, S. (1990). Fault-propagation folds: Geometry kinematic evolution, hydrocarbon traps. *American Association of Petroleum Geologists Bulletin V*, *74*, 921–945.

Muñoz, J., Troncoso, R., Duhart, P., Crignola, P., Farmer, L., & Stern, C. R. (2000). The relation of the mid-Tertiary coastal magmatic belt in south central Chile to the late Oligocene increase in plate convergence rate. *Revista Geológica de Chile*, *27*(2), 177–203.

Muñoz, N. (1996). The thermal evolution of Jurassic and Cretaceous source rocks in the Malargüe thrust belt, Argentina: Implications for hydrocarbon exploration. Independent project report. Unpublished MSc course in basin evolution and dynamics. Department of Geology. Royal Holloway University of London, p 98.

Naeser, C. W. (1976). Fission track dating, U. S. Geological Survey, 65.

Naipauer, M., Tunik, M., Marques, J. C., Rojas Vera, E. A., Vujovich, G. I., Pimentel, M. M., & Ramos, V. A. (2015). U-Pb detrital zircon ages of Upper Jurassic continental successions: Implications for the provenance and absolute age of the Jurassic-Cretaceous boundary in the Neuquén Basin. In S. Sepúlveda, L. Giambiagi, L. Pinto, S. Moreiras, M. Tunik, G. Hoke, & M. Farías (Eds.), *Geodynamic processes in the Andes of Central Chile and Argentina*. *Geological Society of London, Special Publications, 399*, 131–154.

Nocioni, A. (1996). Estudio estructural de la Faja Plegada y Corrida de la Cuenca Neuquina- Surmendocina. 13° Congreso Geológico Argentino and 3° Congreso de Exploración de Hidrocarburos, Actas 2, 353-372, Buenos Aires.

Ploszkiewicz, V., & R. Viñes (1987). Filo Morado: Un descubrimiento exploratorio en cinturón plegado, Boletín Inf. Pet., 4, 10, 97–102, Buenos Aires.

Radic, J. P. (2010). Las cuencas cenozoicas y su control en el volcanismo de los Complejos Nevados de Chillán y Copahue-Callaqui (Andes del Sur, 36-39°S). *Geology*, *37*, 220–246.

Radic J. P., L. Rojas, A. Carpinelli, & E. Zurita (2002). Evolución Tectónica de la cuenca Terciaria de Cura-Mallín Región Cordillerana Chileno Argentina (36°30′-39°00´S). In: XV Congreso Geológico Argentino, Actas 3, Calafate, pp 233–237.

Ramos, V., & Folguera, A. (2005). Tectonic evolution of the Andes of Neuquén: Constraints derived from the magmatic arc and foreland deformation. In G. Veiga, L. Spalletti, J. Howell, & E. Schwarz (Eds.), *The Neuquén Basin: A case study in sequence stratigraphy and basin dynamics*. *Geological Society of London, Special Publication, 252*, 15–35.

Ramos, V. A. (1998). Estructura del sector occidental de la faja plegada y corrida del Agrio, cuenca Neuquina, Argentina, 10° Congreso Latinoamericano de Geología (Buenos Aires). *Actas*, *2*, 105–110.

Ramos, V. A. (2010). The tectonic regime along the Andes: Present-day and Mesozoic regimes. *Geological Journal*, *45*(1), 2–25. https://doi.org/10.1002/gj.1193

Ramos, V. A., & Barbieri, M. (1989). El volcanismo cenozoico de Huantraico: Edad y relaciones isotópicas iniciales, provincia de Neuquén. *Revista de la Asociación Geológica Argentina*, *43*, 210–223.

Ramos, V. A., & Kay, S. M. (2006). Overview of the evolution of the southern Central Andes of Mendoza and Neuquén (35°-39°S latitude). In S. M. Kay, & V. A. Ramos (Eds.), *Evolution of an Andean margin: A tectonic and magmatic view from the Andes to the Neuquén Basin (35°-39°S Latitude)*. *Geological Society of America, Special Paper, 407*, 1–17.

Ramos, V. A., Litvak, V., Folguera, A., & Spagnuolo, M. (2014). An Andean tectonic cycle: From crustal thickening to extension in a thin crust (34–37°S). *Geoscience Frontiers*, *5*(3), 351–367. https://doi.org/10.1016/j.gsf.2013.12.009

Reiners, P. W. (2005). Zircon (U-Th)/He thermochronometry. *Reviews in Mineralogy and Geochemistry*, *58*(1), 151–179. https://doi.org/10.2138/rmg.2005.58.6

Reiners, P. W., & Brandon, M. T. (2006). Using thermochronology to understand orogenic erosion. *Annual Review of Earth and Planetary Sciences*, *34*(1), 419–466. https://doi.org/10.1146/annurev.earth.34.031405.125202

Reiners, P. W., Carlson, R. W., Renne, P. R., Cooper, K. M., Granger, D. E., McLean, N. M., & Schoene, B. (2018). *Geochronology and thermochronology, American Geophysical Union* (p. 480). Washington, DC: Willey. https://doi.org/10.1002/9781118455876

Reiners, P. W., Spell, T. L., Nicolescu, S., & Zanetti, K. A. (2004). Zircon (U-Th)/He thermochronometry: He diffusion and comparisons with $^{40}Ar/^{39}Ar$ dating. *Geochimica et Cosmochimica Acta*, *68*, 1857–1,1887.

Rojas Vera, E. A., Mescua, J., Folguera, A., Becker, T. P., Sagripanti, L., Fenell, L., et al. (2015). Evolution of the Chos Malal and Agrio fold and thrust belts, Andes of Neuquén: Insights from structural analysis and apatite fission track dating. *Journal of South American Earth Sciences*, *64*(2), 418–433. https://doi.org/10.1016/j.jsames.2015.10.001

Rovere, E. (1998). Volcanismo jurásico, paleógeno y neógeno en el noroeste del Neuquén, Argentina. 10° Congreso Latinoamericano de Geología y 6° Congreso Nacional de Geología Económica, Actas 144-149, Buenos Aires.

Sagripanti, L., Colavitto, B., Jagoe, L., Folguera, A., & Costa, C. (2018). A review about the quaternary upper-plate deformation in the Southern Central Andes (36–38°S): A plausible interactions between mantle dynamics (Pembroke, Ont.) and tectonics. *Journal of South American Earth Sciences*, 1–11. https://doi.org/10.1016/j.jsames.2017.11.008

Sagripanti, L., Folguera, A., Fennell, L., Rojas Vera, E., & Ramos, V. (2016). Progression of the deformation in the southern central Andes. In Folguera et al. (Eds.), *Growth of the southern Andes* (chap. 5, pp. 205–236). Cham, Switzerland: Springer ESS. https://doi.org/10.1007/978-3-319-23060-3_6

Sagripanti, L., Folguera, A., Giménez, M., Rojas Vera, E. A., Fabiano, J. J., Molnar, N., et al. (2014). Geometry of middle to late Triassic extensional deformation pattern in the Cordillera del Viento (southern central Andes): A combined field and geophysical study. *Journal of Iberian Geology*, *40*, 349–366.

Sagripanti, L., RojasVera, E., Gianni, G., Folguera, A., Harvey, J., Farías, M., & Ramos, V. A. (2015). Neotectonic reactivation of the western section of the Malargüe fold and thrust belt (Tromen volcanic plateau, Southern Central Andes). *Geomorphology*, *232*, 164–181.

Sánchez, N., Turienzo, M., Lebinson, F., Araujo, V., Coutand, I., & Dimieri, L. (2015). Structural style of the Chos Malal fold-and-thrust belt, Neuquén Basin, Argentina: Relationship between thick and thin-skinned tectonics, in tectonics of the Argentine and Chilean Andes. *Special Issue Journal of South American Earth Sciences*, *64*, 399–417.

Sánchez, N. P. (2015), Evolución tectónica de las estructuras andinas en la región del río Neuquén (~37°20′ L.S), faja corrida y plegada de Chos Malal, provincia de Neuquén, Tesis Doctoral, Universidad Nacional del Sur, Bahía Blanca, 215 pp. Retrieved from http://repositoriodigital.uns.edu.ar/bitstream/123456789/2364/1/Natalia%20S%C3%A1nchez-%20Tesis%20Doctoral-%202015.pdf

Selva, G., J. Vittone, & G. Vergani (2005). Trampas Estructurales en el Pie de Sierra de la Faja Plegada Neuquina. In: Kozlowski, E., G. Vergani, and A. Boll, (eds.), Las Trampas de Hidrocarburos en las Cuencas Productivas de Argentina, Simposio del 6° Congreso de Exploración y Desarrollo de Hidrocarburos, IAPG, p. 141–156, Buenos Aires.

Shuster, D. L., Flowers, R. M., & Farley, K. A. (2006). The influence of natural radiation damage on helium diffusion kinetics in apatite. *Earth and Planetary Science Letters*, *249*(3-4), 148–161. https://doi.org/10.1016/j.epsl.2006.07.028

Spagnuolo, M., Litvak, V., Folguera, A., Bottesi, G., & Ramos, V. A. (2012). Neogene magmatic expansion and mountain building processes at the southern central Andes, 36°-37°S. *Argentina, Journal of Geodynamics*, *53*, 81–95. https://doi.org/10.1016/j.jog. 2011.07.004

Spalletti, L. A., & Dalla Salda, L. H. (1996). Apull-apart volcanic-related Tertiary Basin: An example from the Patagonian Andes. *Journal of South American Earth Sciences*, *9*(3/4), 197–206. https://doi.org/10.1016/0895-9811 (96)00006-5

Suárez, M., & Emparán, C. (1995). The stratigraphy, geochronologyand paleophysiography of a Miocene freshwater interarc basin, southern Chile. *Journal of South American Earth Sciences*, *8*(1), 17–31. https://doi.org/10.1016/0895-9811(94)00038-4

Suppe, J. (1983). Geometry and kinematics of fault-bend folding. *American Journal of Science*, *283*(7), 684–721. https://doi.org/10.2475/ajs.283.7.684

Suppe, J., & Medwedeff, D. (1990). Geometry and kinematics of fault-propagation folding. *Eclogae Geologicae Helvetiae*, *83*, 409–454.

Tagami, T., & O'Sullivan, P. B. (2005). Fundamentals of fission-track thermochronology. *Reviews in Mineralogy and Geochemistry*, *58*(1), 19–47. https://doi.org/10.2138/rmg.2005.58.2

Tunik, M., Folguera, A., Naipauer, M., Pimentel, M., & Ramos, V. (2010). Early uplift and orogenic deformation in the Neuquén Basin: Constraints on the Andean uplift from U-Pb and Hf isotopic data of detrital zircons. *Tectonophysics*, *489*(1-4), 258–273. https://doi.org/10.1016/j.tecto.2010.04.017

Turienzo, M., Sánchez, N., Dimieri, L., Lebinson, F., & Araujo, V. (2014). Tectonic repetitions of the Early Cretaceous Agrio Formation in the Chos Malal fold-and-thrust belt, Neuquén basin, Argentina: Geometry, kinematics and structural implications for Andean building. *Journal of South American Earth Sciences*, *53*, 1–19. https://doi.org/10.1016/j.jsames.2014.04.004

Turienzo, M., N. Sánchez, F. Lebinson, & L. Dimieri (2015). Consideraciones estructurales sobre la interacción entre el basamento y la cubierta sedimentaria en la región de Pampa Tril–Filo Morado, Cuenca Neuquina. 15° Reunión de Tectónica, General Roca, Acta de Resúmenes, p. 150–151.

Turienzo, M., Sánchez, N., Lebinson, F., & Dimieri, L. (2018). The structure of the southern Central Andes (Chos Malal fold and thrust belt). In: Folguera et al. (Eds), the evolution of the Chilean-Argentinean Andes. *special publication*, *17*, 419–451. https://doi.org/10.1007/978-3-319-67774-3

Vergani, G. D., C. Arregui, & O. Carbone (2011). Sistemas petroleros y tipos de entrapamientos de la Cuenca Neuquina, Relatorio del 18° Congreso geológico la provincia del Nuequén, 645–656, Neuquén.

Vergani, G. D., Tankard, A. J., Bellotti, H., & Welsink, H. J. (1995). Tectonic evolution and paleogeography of the Neuquén Basin, Argentina. Petroleum basins of South America. *America Association of petroleum geologists, Memoir*, *62*, 383–402.

Viñes, R. (1989). Interpretación de la estructura de Filo Morado: 1° Congreso Nacional de Exploración de Hidrocarburos. *Actas*, *2*, 1,107–1,124.

Wagner, G. A., & Van den haute, P. (1992). *Fission track-dating* (285 pp.). Dordrecht: Kluwer Academic. https://doi.org/10.1007/978-94-011-2478-2

Wolf, R. A., Farley, K. A., & Kass, D. M. (1998). Modeling of the temperature sensitivity of theapatite (U-Th)/He thermochronometer. *Chemical Geology*, *148*(1-2), 105–114. https://doi.org/10.1016/S0009-2541(98)00024-2

Zamora Valcarce, G., Rapalini, A., & Spagnuolo, C. (2007). Reactivación de estructuras cretácicas durante la deformación miocena, Faja plegada del Agrio, Neuquén. *Revista de la Asociación Geológica Argentina*, *62*(2), 299–307.

Zamora Valcarce, G., Zapata, T., Ansa, A., & Selva, G. (2006). Three-dimensional structural modeling and its application for development of the El Portón field, Argentina. *American Association of Petroleum Geologists Bulletin*, *90*(3), 307–319.

Zamora Valcarce, G., Zapata, T., Ramos, V. A., Rodríguez, F., & Bernardo, M. L. (2009). Evolución tectónica del frente andino en Neuquén. *Revista de la Asociación Geológica Argentina*, *65*, 192–203.

Zapata, T., Brissón, I., & Dzelalija, F. (1999). La estructura de la faja plegada y corrida andina en relación con el control del basamento de la Cuenca Neuquina. *Boletín de Informaciones Petroleras*, *60*, 113–121.

Zapata, T., Dzelalija, F., & Olivieri, G. (2001). Desarrollo de reservorios fracturados de la Formación Mulichinco usando modelado estructural 3D: Yacimiento Filo Morado, Cuenca Neuquina, Argentina. *Boletín de Informaciones Petroleras*, *66*, 38–47.

Zapata, T. R., & Folguera, A. (2005). Tectonic evolution of the Andean fold and thrust belt of the southern Neuquén Basin, Argentina. In L. Spalletti, G. Veiga, E. Y. Schwarz, & J. Howell (Eds.), *The Neuquén Basin: A case study in sequence stratigraphy and basin dynamics*. *Geological Society of London, Special Publications, 252*, 37–56.

Zöllner, W., & Amos, A. J. (1973). Descripción geológica de la Hoja 32b, Chos Malal, provincia del Neuquén. *Servicio Nacional Minero Geológico, Boletín*, *143*, 1–91.